Associative Memory Models of Hippocampal Areas CA1 and CA3

Bruce P. Graham, Vassilis Cutsuridis, and Russell Hunter

Overview

The hippocampal regions CA3 and CA1 have long been proposed to be auto- and heteroassociative memories, respectively (Marr, 1971; McNaughton and Morris, 1987; Treves and Rolls, 1994), for the storage of declarative information. An autoassociative memory is formed when a set of neurons are recurrently connected by modifiable synapses, whereas a heteroassociative memory is formed through modifiable connections from an input layer of neurons to an output layer. Associative memory storage simply requires a Hebbian strengthening of connections between neurons that are coactive (Amit, 1989; Hopfield, 1982; Willshaw et al., 1969). Recall proceeds from a cue activity pattern across neurons that is a partial or noisy version of a previously stored pattern. A suitable firing threshold on each neuron that receives input from already active neurons ensures that neural activity evolves towards the stored pattern. This may happen with only one or two updates of each neuron's activity. Accurate recall is obtainable provided not too many patterns have been stored, otherwise recall is poor, or even impossible.

Network models of spiking neurons can be used to explore the dynamics of storage and recall in such memory networks. Here we introduce a recurrent network model based on hippocampal area CA3 and a feedforward network model for area CA1. Cells are simplified compartmental models with complex ion channel dynamics. In addition to pyramidal cells, one or more types of interneuron are present. We investigate, in particular, the roles of these interneurons in setting the appropriate threshold for memory recall.

B.P. Graham (✉)
Department of Computing Science and Mathematics, University of Stirling, Stirling FK9 4LA, UK
e-mail: b.graham@cs.stir.ac.ak

V. Cutsuridis et al. (eds.), *Hippocampal Microcircuits*, Springer Series in Computational Neuroscience 5, DOI 10.1007/978-1-4419-0996-1_16,

Associative Memory and the Hippocampus

Pyramidal cells within CA3 form sufficient recurrent connections between themselves that they can putatively operate as an associative memory network (de Almeida et al., 2007; Treves and Rolls, 1994). Patterns of pyramidal cell (PC) activity may largely be determined by mossy fibre inputs from the dentate gyrus (Fig. 1). Such patterns are stored autoassociatively by Hebbian modification of recurrent connections between CA3 PCs (Treves and Rolls, 1994). Patterns of CA1 PC activity may be determined by direct afferent input from the entorhinal cortex (Fig. 1). Temporal correspondence between these patterns and patterns of activity in CA3 PCs results in their heteroassociation in CA1 by modification of CA3 Schaffer collateral synapses onto active CA1 PCs (Hasselmo et al., 2002a).

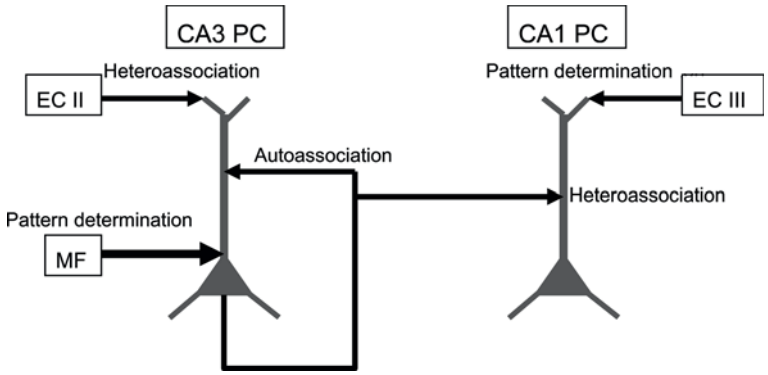

Fig. 1 Associative memory in the hippocampus. Mossy fibre (MF) inputs from the dentate gyrus create pyramidal cell (PC) activity in CA3 that is stored autoassociatively by Hebbian modification of recurrent collateral synapses between coactive PCs. Patterns of activity in layer II of entorhinal cortex (EC II) may be heteroassociated with these CA3 patterns. At the same time, CA1 PCs receiving input both from layer III of entorhinal cortex and from CA3 PCs form a heterassociation with the active CA3 PCs through Hebbian modification of the Schaffer collateral synapses

Gamma frequency rhythms (30–100 Hz) are assumed to constitute a basic clock cycle such that patterns of activity for storage and recall correspond to PCs that are active in a particular gamma cycle (Axmacher et al., 2006; Buzsaki and Chrobak, 1995; Lisman and Idiart, 1995). The slower theta rhythm (4–10 Hz) is assumed to modulate episodes of storage of new information and recall of old information in its half cycles (Hasselmo et al., 2002a, b). During exploration an animal is likely to encounter both familiar and novel situations. Storage of new episodes with minimal interference from already encoded episodes takes place most efficiently if storage and recall are temporally separated in the encoding neural networks (Wallenstein and Hasselmo, 1997). Waxing and waning of GABA-mediated inhibition from the medial septum lead alternately to disinhibition and inhibition of PCs during a theta cycle, corresponding to ideal conditions for pattern recall and pattern storage, respectively. In the results to follow, we only consider the

recall phase. Results on modelling both storage and recall in CA1 can be found in Cutsuridis et al. (2007, 2008a, 2009a) and Cutsuridis and Wennekers (2009). Other models consider storage and recall in CA3 (Kunec et al., 2005; Wallenstein and Hasselmo, 1997).

Hebbian Pattern Storage and Recall

Rather than considering the biological requirements for pattern storage via induction of long-term potentiation (LTP), patterns are stored in our networks by generating a weight matrix using a Hebbian learning rule (the reader is referred to Cutsuridis and colleagues (2008a, 2009a, 2009) for an example of using a spike timing-dependent plasticity rule to store patterns). These weights are then used to set the conductance strengths of AMPA synapses between PCs. Patterns are specified as binary vectors, which represent the activity (1) or silence (0) of each PC. A clipped Hebbian rule is used to generate a binary weight matrix, where an entry of 1 at index (i,j) indicates that the PCs i and j, where i connects onto j, were both active in the same pattern during storage. An example weight matrix that results from the storage of two patterns in an autoassociative memory (or, equivalently, a heteroassociative memory in which the input and output patterns are identical) is illustrated in Fig. 2a.

In an artificial neural network implementation with binary computing units, recall of a previously stored pattern proceeds by multiplying a cue pattern (full, partial or noisy version of a stored pattern) with the weight matrix to give the weighted sum

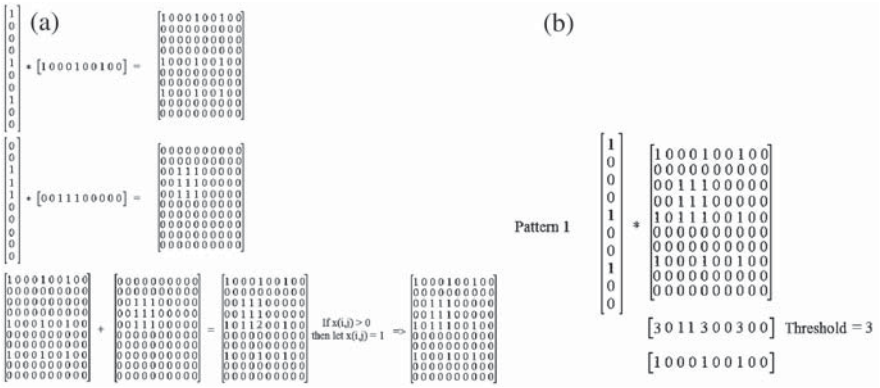

Fig. 2 (**a**) Weight matrix from the autoassociative storage of two patterns via clipped Hebbian learning. The individual weight matrices from the individual storage of the patterns are simply obtained as the outer product of the pattern with itself. The combined weight matrix is obtained by summing the individual matrices and then clipping entries to be 0 or 1. (**b**) Pattern recall strategy. The cue pattern is multiplied with the weight matrix to give a vector of weighted input sums. This vector is thresholded to give the recalled binary vector. With the noiseless cue illustrated here, a suitable threshold is simply the number of active units in the cue pattern

of the inputs to each cell in the network. Recall then involves thresholding these weighted sums to create an output pattern that contains 1 s for all those cells that are receiving the highest input sums. This output pattern will equal the stored cue pattern if recall is error-free. To give an example, we use the weight matrix in which the two patterns shown in Fig. 2a have been stored. The first of these patterns is used as the recall cue. The input column vector (cue pattern 1) is multiplied with the weight matrix to give the output row vector which is the weighted input sums to each of the 10 cells in the network (Fig. 2b). This vector is [3 0 1 1 3 0 0 3 0 0]. It is easily seen that the highest sums (3) are all to the cells that belong to the stored cue pattern. Some other cells get a lower input of 1, since the two stored patterns overlap with each other. Recall proceeds by applying an activity threshold, and in this case a threshold of 3 is appropriate. The final output activity vector is determined by making active (vector entry 1) all those cells whose input sum is greater than or equal to the threshold (3), else the vector entry is 0. The new output vector after the threshold setting is applied is [1 0 0 0 1 0 0 1 0 0], which is identical to the input vector. Therefore the pattern has been successfully recalled.

More challenging scenarios are when a noisy or partial cue is applied to the network, or when the network is only partially connected (that is, not all neurons are connected to all other neurons, which is typical in biological neural nets). Then the appropriate threshold on the input sums is not so easily chosen. One rule is to chose a threshold that will guarantee the expected number of cells are active in the output pattern (this does not, however, guarantee that they are the correct cells!)

In the scenario of spiking neurons, this thresholding process involves the intrinsic action potential generation threshold of a neuron and its modulation by such factors as inhibition. Weighted input sums are now the summation of EPSPs of differing amplitude generated by action potentials from active input neurons arriving at roughly the same time at different excitatory synapses. If the summed EPSPs, which may be inhibited, cause the membrane potential of the axon initial segment to reach threshold, then the cell fires an action potential and is deemed to be active.

The models that follow explore this process in detail for partially connected autoassociative and heteroassociative networks of spiking neurons.

The Models

Autoassociative Memory in CA3

The principal excitatory cells of the CA3 region are pyramidal cells. These cells are driven by inputs from the dentate gyrus and entorhinal cortex, and may have sufficient recurrent connectivity to act as an autoassociative memory (de Almeida et al., 2007; Treves and Rolls, 1994). We construct a recurrent neural network model consisting of a large number of pyramidal cells (PCs) and a smaller number

of inhibitory neurons (putative basket cells). Connectivity between PCs is determined by a connectivity matrix derived from storing patterns using Hebbian learning as described above. Inhibitory connectivity is tuned to achieve accurate recall of a stored pattern when a few of the PCs belonging to a particular stored pattern are given tonic stimulation to make them active and thus act as a recall cue. This model is an extension of the Sommer and Wennekers work (2000, 2001) in which now a number of explicit, spiking interneurons provide the inhibition (Hunter et al., 2008a, b, 2009).

The CA3 Network

The network contains 100 pyramidal cells (PCs), whose interconnectivity is determined by a random pattern of physical connections plus the setting of connection weights as determined by Hebbian learning of stored activity patterns. To represent our learnt binary weights, all AMPA synapses are given the same maximum conductance value. A fully connected PC network involves an individual PC connecting to every other PC, but not to itself, giving n^2–n physical connections, where n is the number of PCs in the network. Full connectivity is not biologically realistic, but serves as a control case for examining the effects of missing connections on memory performance. In CA3, recurrent connections between PCs are numerous, but still sparse, with a single PC receiving connections on average from around 10% of other PCs (Ishizuka et al., 1990; Li et al., 1994). In the model network, partial connectivity is achieved by random deletion of possible connections, without any topographical considerations of relative PC spatial positions. This is a reasonable first approximation to connectivity within a subpart of CA3 (de Almeida et al., 2007; Ishizuka et al., 1990; Li et al., 1994).

Individual PCs are modelled using the tried-and-tested two-compartment model of Pinsky and Rinzel (1994). This model is sufficient to reproduce regular spiking and bursting behaviour in these cells, and to provide a spatial separation of inputs to the dendrites from inputs to the soma.

The somatic compartment contains fast sodium and delayed-rectifier potassium currents. The dendritic compartment contains a calcium current and two (fast and slow) calcium-activated potassium currents. The two compartments are joined by a coupling conductance. Slow calcium spikes and their termination by the calcium-activated potassium currents can generate burst firing in this cell model. Inhibition in the network is provided by fast-spiking basket cells (BCs). A small compartmental model is used that is derived from experimental data on such cells in the dentate gyrus (Santhakumar et al., 2005). Full details of both cell models are given in Appendix 1.

The network model of Sommer and Wennekers (2000, 2001) used "pseudo-inhibition", in which each PC also provided an inhibitory connection onto all other PCs, so that each PC received inhibition in proportion to the amount of PC activity. Explicit interneurons were not modelled. Here, explicit inhibitory circuitry is included in two configurations (Hunter et al., 2009):

1. A single inhibitory interneuron (basket cell - BC) is driven by all pyramidal cells and feeds back inhibition to all PCs equally (Fig. 3a).
2. The network contains 100 BCs, each of which is driven by a single PC, but all of which feedback inhibition to all PCs (Fig. 3b).

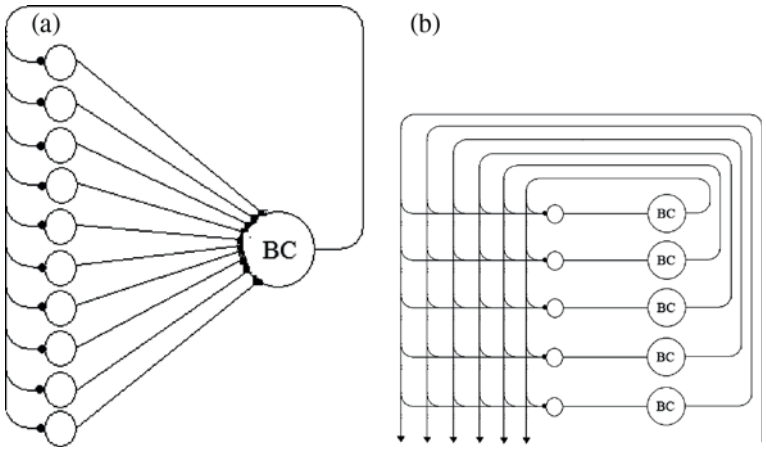

Fig. 3 Two network configurations with explicit inhibitory basket cells (BC) that act to modify PC firing thresholds. (**a**) One inhibitory interneuron that is driven equally by all PCs and feeds back inhibition to all PCs. (**b**) One interneuron (BC) for each PC, with each BC being driven by a single PC, but feeding back inhibition to all PCs

The first configuration provides inhibition that is relatively constant, provided that sufficient PCs are active to cause the BC to spike. The BC spiking rate is only a moderate function of PC activity. In the second configuration, the amount of inhibition projected to each PC is a strong function of the current PC activity level across the network. This should be closest to the "pseudo-inhibition" of Sommer and Wennekers (2000, 2001). The purpose of these configurations is to determine whether it is necessary for inhibition to accurately reflect PC activity levels for accurate pattern recall.

Pattern Recall in CA3

To test recall in these networks, 50 random patterns, each consisting of 10 active PCs, were stored in the network using the Hebbian learning procedure described above. Then 5 PCs from a given pattern were stimulated using a constant current injection to cause them to fire and act as a recall cue. Network activity was monitored over a period of time to see if the remaining PCs of the stored pattern, or other PCs became active through the recurrent connections from the cued PCs.

With no inhibition in the network, most PCs become activated and so it cannot be said that the stored pattern is recalled. However, as illustrated in Fig. 4, a suitable level of inhibition results in reasonably accurate recall of the stored pattern. In Fig. 4a the network contains the "pseudo-inhibition" of Sommer and Wennekers

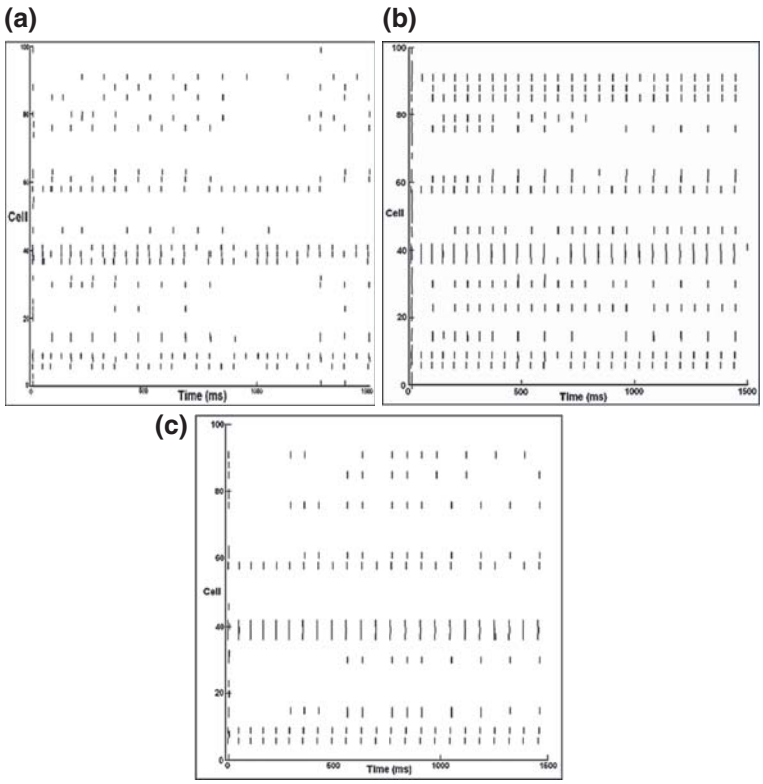

Fig. 4 Raster plots of pyramidal cell activity during recall over 1,500 ms in a partially connected (10%) net. (**a**) Pseudo-inhibition, (**b**) 1 BC, (**c**) 100 BCs

(2000, 2001). Now most active cells either belong to the cue or to the stored pattern. This is a partially connected network, which introduces noise into the recall procedure and results in occasional spurious firings of non-pattern PCs. Recall activity proceeds at around 20 Hz, at the low end of the gamma frequency range. Figure 4b, c illustrates recall with networks that include explicit interneurons. Recall dynamics and quality are very similar to the "pseudo-inhibition" case, irrespective as to whether there is a single inhibitory interneuron, or whether there is 100 INs. Thus it seems that recall is rather robust to the precise level of inhibition and whether or not it is in proportion to the PC activity level (which is relatively constant in these examples).

Heteroassociative Memory in CA1

In this section we describe a more detailed model, this time of the CA1 microcircuitry (Fig. 5). The principal excitatory cells of the CA1 region also are pyramidal cells. These cells are driven by excitatory inputs from layer III of the entorhinal cortex and the CA3 Schaffer collaterals and an inhibitory input from

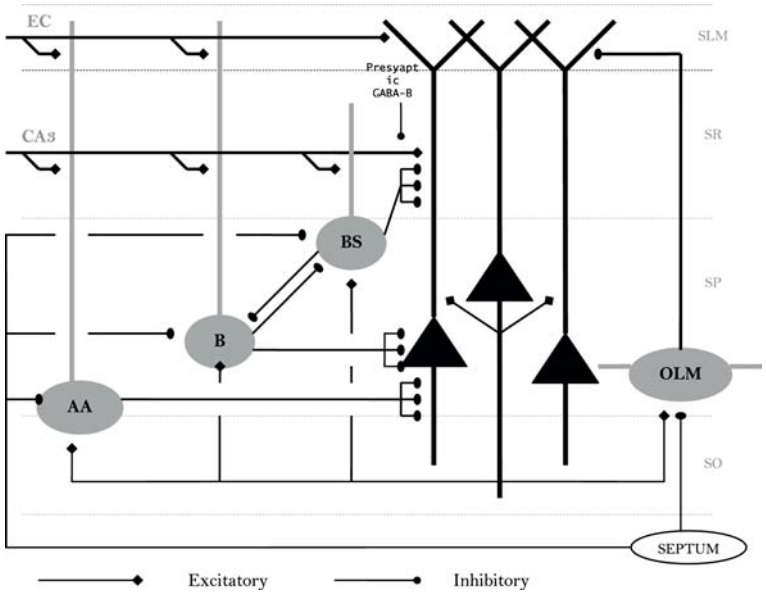

Fig. 5 Hippocampal CA1 microcircuit showing major cell types and their connectivity. *Black filled triangles*: pyramidal cells. *Grey filled circles*: CA1 inhibitory interneurons. EC: entorhinal cortex input; CA3: CA3 Schaffer collateral input; AA: axo-axonic cell; B: basket cell; BS: bistratified cell; OLM: oriens lacunosum-moleculare cell; SLM: stratum lacunosum-moleculare; SR: stratum radiatum; SP: stratum pyramidale; SO: stratum oriens. *Open circles*: Septal GABA inhibition. (Reproduced with permission from Cutsuridis et al. (2009a), Fig. 1, Copyright Wiley-Blackwell.)

the medial septum. Recurrent connectivity between pyramidal cells is negligible in CA1 (less than 1%). We construct a feedforward neural network model consisting of pyramidal cells and four types of inhibitory interneurons: basket cells, axo-axonic cells, bistratified cells and oriens lacunosum-moleculare cells. As with the CA3 model, a connectivity matrix is derived by storing patterns using Hebbian learning, as described above. This matrix is used to specify connectivity from CA3 PCs onto CA1 PCs, forming an excitatory feedforward network. Inhibitory connectivity is tuned to achieve accurate recall of stored patterns when CA3 PCs belonging to a particular stored pattern are active and thus act as a recall cue. Preliminary versions of this model has been published previously in Cutsuridis et al. (2007, 2008a), in Graham and Cutsuridis (2009) and in its complete form in Cutsuridis et al. (2009a) and Cutsuridis and Wennekers (2009).

The CA1 Network

The network contains 100 pyramidal cells (PC), 2 basket cells (BC), 1 bistratified cell (BSC), 1 axo-axonic cell (AAC) and 1 oriens lacunosum-moleculare (OLM) cell (see Fig. 5). All cell morphologies included a soma, apical and basal dendrites and a portion of axon. The dimensions of the somatic, axonic and dendritic

compartments of the model cells are presented in Table 3. The biophysical properties of each cell were adapted from cell types reported in the literature (Poirazi et al., 2003a, b; Saraga et al., 2003; Santhakumar et al., 2005). The complete mathematical formalism of the model is described in Appendix 2. The parameters of all passive and active ionic conductances used in the model are listed in Tables 4, 5, and 6. The synaptic waveform parameters are given in Table 7 and synaptic conductances are listed in Table 8.

Synaptic properties: In the model, AMPA, NMDA, GABA-A and GABA-B synapses are considered. GABA-A is present in all strata, whereas GABA-B is present in medium and distal SR and SLM dendrites. AMPA synapses are present in strata LM (EC connections) and radiatum (CA3 connections), whereas NMDA are present only in stratum radiatum (CA3 connections).

Model inputs: Inputs to the CA1 model come from the medial septum (MS), entorhinal cortex (EC) and CA3 Schaffer collaterals. The EC input is modelled as the firing of 20 entorhinal cortical cells at an average gamma frequency of 40 Hz (spike trains only modelled and not the explicit cells), and the CA3 input is modelled with the same gamma frequency spiking of 20 out of 100 CA3 pyramidal cells (see Appendix 2 for details). PCs, BCs, AACs, BSCs received CA3 input in their medial SR dendrites, whereas PCs, BCs and AACs received also the EC layer III input in their apical LM dendrites. EC inputs preceded CA3 inputs by 9 ms on average, in accord with experimental data showing that the conduction latency of the EC-layer III input to CA1 LM dendrites is less than 9 ms (ranging between 5 and 8 ms), whereas the conduction latency of EC-layer II input to CA1 radiatum dendrites via the di/tri-synaptic path is greater than 9 ms (ranging between 12 and 18 ms) (Leung et al., 1995; Soleng et al., 2003). MS input, which is modelled as the rhythmic firing of 10 septal cells (see Appendix 2 for details), provides GABA-A inhibition to all INs in the model (strongest to BC and AAC; Freund and Antal, 1988). MS input is phasic at theta rhythm and is on for 125 ms during the retrieval phase.

Presynaptic GABA-B inhibition: It has been shown that the strengths of the synaptic inputs from the EC perforant path and the CA3 Schaffer collaterals wax and wane according to the extracellular theta rhythm and 180° out of phase from each other (Brankack et al., 1993; Wyble et al., 2000). These cyclical theta changes are likely due to the presynaptic GABA-B inhibition to CA3 Schaffer collateral input to CA1 PCs' synapses, which is active during the storage cycle and inactive during recall (Molyneaux and Hasselmo, 2002). This is modelled simply as a reductive scaling during storage of the CA3-AMPA synaptic conductance, so that the effective conductance g' is

$$g' = g_s \cdot g \tag{1}$$

where g_s is the scaling factor (set to 0.4 in the presented simulations). During recall, g' is simply equal to g (the AMPA conductance determined by the connectivity weight matrix).

Pattern Recall in CA1

Hasselmo and colleagues (2002a, b) have hypothesized that the hippocampal theta rhythm (4–7 Hz) contributes to memory formation by separating storage and recall into different functional subcycles. Recent experimental evidence has shown that different types of inhibitory interneurons fire at different phases of the theta rhythm (Klausberger et al., 2003, 2004; Somogyi and Klausberger, 2005; Klausberger and Somogyi, 2008). Here, we demonstrate how the recall performance of previously stored patterns is affected by the presence/absence of various types of inhibitory interneurons, which fire at different phases of the simulated theta rhythm (Paulsen and Moser, 1998). A larger set of recall performance and memory capacity results can be found in Cutsuridis et al. (2009a).

As detailed previously, a set of patterns are stored by generating a weight matrix based on a clipped Hebbian learning rule, and using the weight matrix to prespecify the CA3 to CA1 PC connection weights. To test recall of a previously stored pattern, the associated input pattern is applied as a cue in the form of spiking of active CA3 inputs (those belonging to the pattern) distributed within a gamma frequency time window. The entire cue pattern is repeated at gamma frequency (40 Hz). At the same time, 20 EC inputs also fire randomly distributed within a 25 ms gamma window, but with mean activity preceding the CA3 activity by 9 ms. The CA3 spiking drives the CA1 PCs plus the B, AA and BS interneurons. The EC input also drives the B and AA interneurons.

To test pure recall by the CA3 input cue, the EC input is disconnected from the CA1 PCs and no learning takes place at CA3 synapses on CA1 PCs. The CA3 synapses are suppressed during the "storage" phase of theta. Pattern recall only occurs during the "recall" half-cycle. Typical firing patterns of the different cell types across theta cycles are illustrated in Fig. 6.

The recall of the first pattern in a set of five is shown in Fig. 7. Figure 7a shows a raster plot of the spiking of the septal (top 10 rows), EC (next 20 rows) and CA3 (bottom 100 rows) inputs. The remaining subplots show raster plots of CA1 PC activity for different configurations of network inhibition. Figure 7b shows CA1 activity with all inhibitory pathways present. The CA1 PCs are active two or three times during a theta recall cycle, with their spiking activity being a very close match to the stored pattern. Only occasional spurious firings are seen (see recall events at 900, 1,350 and 1,850 ms). Seven recall cycles are shown, following an initialization period of 200 ms.

To test the influence of the inhibitory pathways on recall, different pathways are selectively removed. Bistratified cell inhibition to the medial SR PC dendrites is hypothesized to mediate thresholding of PC firing during recall. Removal of BC and AAC inhibition does not spoil recall quality (Fig. 7c), as they both fire 180° out of phase with respect to the bistratified cells (Klausberger and Somogyi, 2008). Removal of all inhibitory pathways leads to gamma frequency firing of virtually all PCs during recall cycles and the CA3 cued pattern during storage cycles (Fig. 7d). In this latter case, without BC and AAC inhibition, the suppressed CA3 input in a storage cycle is still strong enough to fire the pattern cells, but not the non-pattern cells.

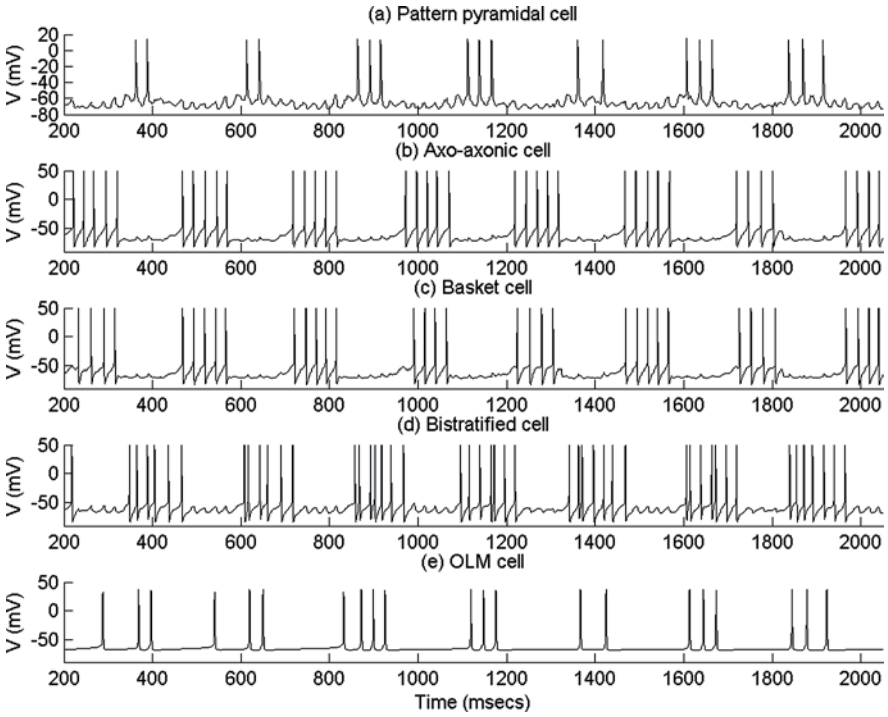

Fig. 6 Voltage traces in an example of a PC belonging to the pattern, and each type of inhibitory interneuron, for the recall episodes in the full network shown in Fig. 7b. (Reproduced with permission from Cutsuridis et al. (2009a), Fig. 10, Copyright Wiley-Blackwell.)

What happens to recall when the EC input is present in CA1 PCs? The EC input corresponding to the cued pattern could potentially aid recall. With such EC input, the pattern is now nearly perfectly recalled on each gamma cycle during a recall theta half-cycle, with occasional spurious firings (Cutsuridis et al., 2009a). OLM inhibition is hypothesized to remove interference from spurious EC input during recall. If the EC input is taken to be due to a different pattern from that of the CA3 input cue, i.e. CA1 PCs receiving the EC input may or may not belong to the cued pattern, then recall is disrupted by the spurious EC input, but this disruption is significantly worse if the OLM inhibition is absent (Cutsuridis et al., 2009a).

Justification

The hypothesis of associative memory function in the subsystems of the hippocampus cannot yet be tested by direct experiments. It is technically not possible to instantiate specific patterns of neural activity for either storage or subsequent recall. That such a process does take place is based on the suitability of the network architecture and evidence from tissue slice experiments of the Hebbian induction

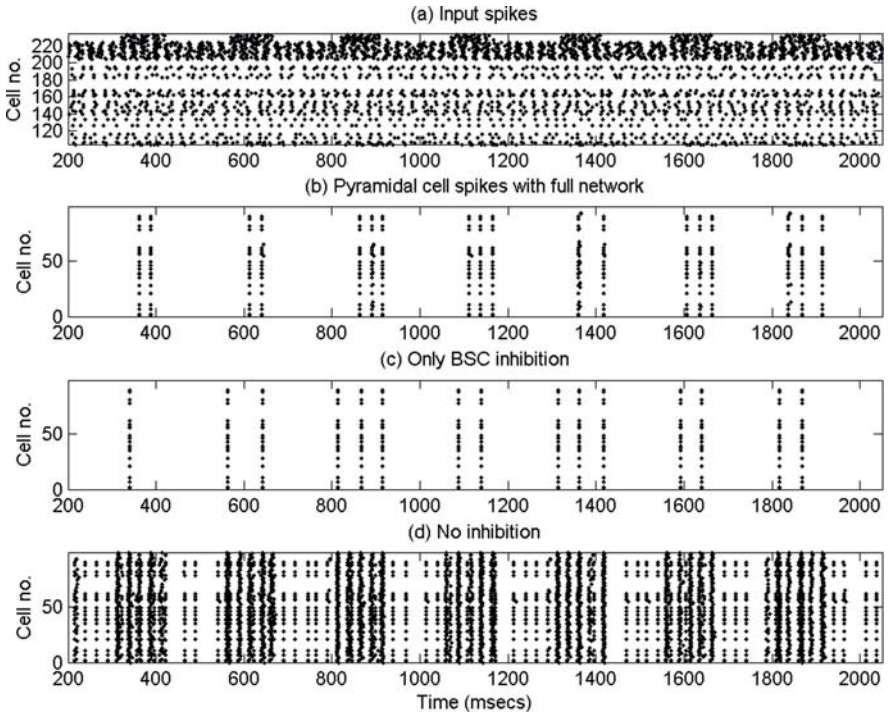

Fig. 7 Example of pattern recall in CA1. The CA3 input is cueing the first pattern in a stored set of five. EC input is present to drive the inhibitory interneurons, but is disconnected from the CA1 PCs, so that recall is purely due to the CA3 input cue. Seven 125 ms recall half-cycles are shown, starting at 300 ms (interspersed with 125 ms storage half-cycles, but STDP is turned off) (**a**) Raster plot showing the septal (*top* 10), EC (*next* 20) and CA3 input (*bottom* 100) spikes. (**b**) Raster plot showing CA1 PC activity – virtually the only active cells are those belonging to the stored pattern. (**c**) BC and AAC inhibition removed, so that recall is mediated only by BSC inhibition. (**d**) BSC and OLM inhibition also removed. (Reproduced with permission from Cutsuridis et al. (2009a), Fig. 9a, b and 11c, d, Copyright Wiley-Blackwell.)

of long-lasting changes in synaptic strength at the relevant connections (Bliss et al., 2007; Mellor, this volume). Behavioural experiments in mammals, including humans, implicate the hippocampus in the intermediate-term storage of episodic memories (see Eichenbaum, this volume). Thus we must rely on computational models to assess the recall and storage abilities of the neural subnetworks of the hippocampus. The models presented here are devised to address the specific issue of whether network inhibition provides suitable control of pyramidal cell activity to allow the successful recall of previously stored patterns. They build upon a variety of models that include different levels of biological realism in exploring associative memory function in the hippocampus (Kunec et al., 2005; Levy, 1996; Menschik and Finkel, 1998; Sommer and Wennekers, 2001; Wallenstein and Hasselmo, 1997). The advance from previous models is to test explicitly the roles during pattern recall

of defined populations of inhibitory interneurons that make specific spatial contacts onto pyramidal cells.

These network models are based upon identified cell types and their known connectivity. Cells of a particular type make connections to other cells at specific spatial locations on the receiving cell, according to the pre- and post-synaptic cell types. Connection probabilities are assumed to be uniform throughout a network, so that there are no spatial gradients in connectivity. Though we refer to these models as being of areas CA3 and CA1, it is better to consider them as models of subsets of these areas. Inter- and intra-areal connectivity does vary along the transverse and longitudinal axes of the hippocampus (Amaral and Witter, 1989; Amaral and Lavenex, 2007; Ishizuka et al., 1990; Li et al., 1994). Sufficient recurrent connectivity for autoassociative memory function may be restricted to subregion CA3a (de Almeida et al., 2007).

All cell models are derived from previously published models of the representative cell types. In turn, these published models are based on known anatomical and electrophysiological data. As detailed in the earlier chapters in the Computational Analysis section of this book, development of such models has reached a considerable degree of sophistication, but any given model still cannot be considered to be the complete and final model of a particular cell type. Simple, but multicompartmental cell anatomies are used here, which allow suitable spatial distributions of ion channels and segregation of synaptic inputs, while minimizing the computational load. The network behaviour studied here is rather robust to the precise details of the individual cell models.

With our autoassociative memory model of area CA3 we have tested whether feedback inhibition during recall needs to accurately reflect pyramidal cell (PC) activity (Hunter et al., 2009). A given basket cell (BC) is driven by many, but not all pyramidal cells in the surrounding network. The firing rate of a BC will be a function of the neural activity level in a sample of pyramidal cells. Thus neural activity across the population of BCs should be proportional to activity in the PC population. However, BCs are known to synchronize their firing through mutual inhibition and gap junction connections (Bartos et al., 2007). This leads to the possibility that the BC network acts more like a single, powerful BC that is activated by the entire population of PCs. In this case the main indicator of the level of PC activity would be the BC firing rate, which may be only moderately modulated by changes in PC activity. Here we tested the two extreme cases of a network with only a single BC driven by all PCs and a network with the same number of BCs as PCs, with each BC being driven by a single PC. The reality is somewhere between these extremes. In any case, the models demonstrate that recurrent inhibition is sufficient to effectively threshold PCs for accurate pattern recall and to maintain fairly constant PC activity levels. The consequence of this is that only a relatively constant level of inhibition is required, which can be provided by either network configuration. Thus the pattern recall process is rather robust to the precise connectivity of the feedback inhibitory network.

The heteroassociative memory model of CA1 is more detailed, containing four types of inhibitory interneuron (axo-axonic, basket, bistratified and oriens

lacunosum-moleculare cells) that form specific feedforward and feedback inhibitory circuits with spatially separated contacts onto PCs (Cutsuridis et al., 2009a). We have used this model to test the hypothesis that storage and recall of patterns can be temporally separated into successive theta rhythm half-cycles (Hasselmo et al., 2002a, b). In vivo recordings have determined that the different classes of interneuron are most active during distinct phases of theta (Klausberger et al., 2003, 2004; Somogyi and Klausberger, 2005; Klausberger and Somogyi, 2008). In particular, bistratified and O-LM cells are most active during the putative recall half-cycle, whereas basket and axo-axonic cells are most active during storage half-cycles. Thus we hypothesize that PC activity during recall is thresholded by inhibition to the proximal dendrites as provided by bistratified cells, rather than by perisomatic inhibition from basket cells. The model results clearly indicate that bistratified cell inhibition can indeed provide appropriate thresholding. In addition, feedback inhibition from O-LM cells can reduce interference to pattern recall from spurious entorhinal cortical inputs to PC distal dendrites. In further work (Cutsuridis et al., 2009a), we have shown that BC and AAC activity, combined with BSC and O-LM inactivity, during a storage half-cycle can effectively block PC output from the soma, while allowing sufficient dendritic excitability due to EC inputs to drive the activity-dependent changes in synaptic strength required for pattern storage. In summary, our model demonstrates that the phasic responses of different classes of inhibitory interneuron seen with in vivo recordings are compatible with the hypothesis that pattern storage and recall occur in separate theta half-cycles. Different IN pathways mediate control of PC activity thresholding and synaptic plasticity (Paulsen and Moser, 1998).

The Future

All aspects of the models we have presented are subject to refinement on the basis of current and future experimental data. This includes cell characteristics, cell types, network connectivity and synaptic strengths and their modification. Fine details of cellular anatomy and ion channel distributions may impact upon signal integration in cells and subsequent cell output. Computational modelling has been vital for examining signal integration in dendrites (Cook and Johnston, 1997; Graham, 2001; Kali and Freund, 2005; Migliore et al., 2005; Poirazi et al., 2003a, b). For example, the oblique dendrites of pyramidal cells may perform local, nonlinear processing of their inputs before integration in the apical trunk on the way to the soma (Poirazi et al., 2003a, b). Backpropagation of action potentials into obliques, which may be required for synaptic plasticity, is strongly influenced by local active membrane properties (Migliore et al., 2005). Further structure in the anatomy of our PC models would be required to capture these aspects, at the cost of computational expense. Nonetheless, these details will likely impact upon memory capacity and recall quality (Graham, 2001).

It is already well known that the inhibitory interneurons within CA3 and CA1 are incredibly diverse, with at least 16 different classes that can be identified

on morphological, electrophysiological and pharmacological grounds (Freund and Buzsaki, 1996; Maccafferi and Lacaille, 2003; Somogyi and Klausberger, 2005). Our CA1 model includes only four classes of inhibitory interneuron. It is clearly a major challenge to develop models that enable the definition and exploration of the function of these many different types of interneuron within the operating neural network. They are likely to provide further fine control of signal integration and synaptic plasticity in pyramidal cells, and may be variously active in different behavioural states of an animal (Axmacher et al., 2006; Klausberger and Somogyi, 2008). With our CA3 network model we are exploring the ability of particular architectures of inhibitory network to improve recall quality in partially connected networks of PCs (Hunter et al., 2008a, b, 2009).

An obvious extension to the models presented here is to explore pattern storage through the use of a suitable learning rule that captures the properties of long-term potentiation (LTP) and depression (LTD) at the pyramidal cell synapses. Here we have generated long-term synaptic strengths using a simple Hebbian learning rule, and these strengths are imposed upon the network when it is instantiated. A rule that could modify synaptic strengths on the basis of ongoing neural activity would allow the exploration of the dynamics of both storage and recall in the same network. An initial exploration in this direction shows that a spike-timing-dependent plasticity (STDP) rule based on the amplitude of postsynaptic voltage transients can be used to store patterns in these memory networks, and that such a pattern can subsequently be successfully recalled (Cutsuridis et al., 2009a). Inclusion of such learning rules within these network models also allows for the investigation of how learning can be modified by intrinsic cell properties and by the timing of inhibitory inputs directed to dendritic locations adjacent to the modifiable synapse (Cutsuridis et al., 2008b, 2009b, c; Paulsen and Moser, 1998; Sjostrom et al., 2008).

Other pathways in these networks are also modifiable, particularly the entorhinal input to the distal dendrites of CA1 PCs (Remondes and Schuman, 2002). Such modifiability could be included in the models via an STDP rule at these synapses. However, an hypothesis as to what information is being learnt, or stored, in this way is required. As discussed below, it seems likely that EC input also plays a significant role in determining CA1 output, which may be underpinned by the heteroassociation of patterns of EC activity with CA1 activity. The strength of inhibition is also modifiable through changes in the strength of excitatory synapses onto inhibitory interneurons. Learning rules at these synapses may be quite different, for example, anti-Hebbian (Lamsa et al., 2007). Network dynamics, and consequent storage and recall of patterns, are also affected by short-term changes in synaptic strength, on time scales of milliseconds to seconds (Sun et al., 2005).

Finally, our models look at information storage and retrieval in isolated hippocampal areas. They do not address the larger questions of information representation, recoding and flow through the hippocampus as a whole (Treves and Rolls, 1994). An assumption of our CA1 model is that EC input is largely responsible for instantiating a pattern of CA1 activity to be associated with a concurrent pattern of CA3 activity through modification of the Schaffer collateral synapses from CA3 PCs onto CA1 PCs. However, CA1 can still maintain sensory coding,

in so-called place cells, without the presence of CA3 (Brun et al., 2002), leading to the view that the direct EC input to CA1 is a major determinant of CA1 output, which may be modulated by the inputs via CA3 (Guzowski et al., 2004; Knierim et al., 2006). In this case the EC input may still contribute to pattern association between CA3 and CA1, but is at the same time determining CA1 spiking activity for output from the hippocampus. Given that EC inputs arrive at the distal apical dendrites of CA1 PCs, it is unclear how much effect they can have on PC spiking. Modelling studies indicate that dendritic spiking, driven by sodium or calcium currents, is crucial to the efficacy of EC inputs in generating output spiking (Kali and Freund, 2005). Since dendritic spiking may also contribute to synaptic plasticity (Golding et al., 2002), this allows for the possible dual role of EC input. There is also a significant inhibitory input to the PC apical dendrites associated with the EC input, the timing of which has significant effects on the efficacy and plasticity of CA3 inputs (Pissadaki and Poirazi, 2007; Remondes and Schuman, 2002).

In summary, computational neural network models of biophysically realistic neurons are invaluable in studying information processing, such as associative memory storage and retrieval, in hippocampal circuits. They are built upon available experimental data and allow the exploration of issues that currently are beyond the scope of experiments with real neural tissue.

Appendix 1: CA3 Cell Models

CA3 Pyramidal Cell Model

The model pyramidal cell is the two-compartment minimal model proposed by Pinsky and Rinzel (1994), that reproduces the essential spiking characteristics, including bursting behaviour, of CA3 pyramidal cells. The current balance equations for the two compartments (soma: s and dendrite: d) are

$$C_{\mathrm{m}}\frac{dV_{\mathrm{s}}}{dt} = -I_{\mathrm{leak}}(V_{\mathrm{s}}) - I_{\mathrm{Na}}(V_{\mathrm{s}}) - I_{\mathrm{K\text{-}DR}}(V_{\mathrm{s}}) + \frac{g_{\mathrm{c}}}{p}(V_{\mathrm{d}} - V_{\mathrm{s}}) + \frac{I_S}{p}$$

$$C_{\mathrm{m}}\frac{dV_{\mathrm{d}}}{dt} = -I_{\mathrm{leak}}(V_{\mathrm{d}}) - I_{\mathrm{Ca}}(V_{\mathrm{d}}) - I_{\mathrm{K\text{-}AHP}}(V_{\mathrm{d}}, \mathrm{Ca}) - I_{\mathrm{K\text{-}C}}(V_{\mathrm{d}}, \mathrm{Ca}) - \frac{I_{\mathrm{syn}}}{(1-p)} + \frac{g_{\mathrm{c}}}{(1-p)}(V_{\mathrm{s}} - V_{\mathrm{d}}) + \frac{I_{\mathrm{d}}}{(1-p)}$$

The two compartments are connected by a coupling conductance, g_{c}, and have relative surface areas specified by p.

The active ionic currents in the soma are

I_{Na} – inward sodium current
$I_{\mathrm{K\text{-}DR}}$ – outward delayed-rectifier potassium current

In the dendrite the active currents are

I_{Ca} – inward current and is carried by calcium and its activation, s, is fast.
$I_{\text{K-C}}$ – calcium-activated potassium current and is proportional to a fast activation variable, c, times a saturating function, $\chi(\mathrm{Ca})$.
$I_{\text{K-AHP}}$ – has a slow activation variable q which is calcium dependent.

There is also a synaptic current, I_{syn}, which is a constant injected current.
The active ionic currents are given by the following equations:

$$
\begin{aligned}
I_{\mathrm{leak}}(V_{\mathrm{s}}) &= \overline{g}_{\mathrm{L}}(V_{\mathrm{s}} - V_{\mathrm{L}}) \\
I_{\mathrm{leak}}(V_{\mathrm{d}}) &= \overline{g}_{\mathrm{L}}(V_{\mathrm{d}} - V_{\mathrm{L}}) \\
I_{\mathrm{Na}}(V_{\mathrm{s}}) &= \overline{g}_{\mathrm{Na}} m_{\infty}^{2}(V_{\mathrm{s}}) h (V_{\mathrm{s}} - V_{\mathrm{Na}}) \\
I_{\text{K-DR}}(V_{\mathrm{s}}) &= \overline{g}_{\text{K-DR}} n (V_{\mathrm{s}} - V_{\mathrm{K}}) \\
I_{\mathrm{Ca}}(V_{\mathrm{d}}) &= \overline{g}_{\mathrm{Ca}} s^{2} (V_{\mathrm{d}} - V_{\mathrm{Ca}}) \\
I_{\text{K-C}}(V_{\mathrm{d}}, \mathrm{Ca}) &= \overline{g}_{\text{K-C}} c \chi(\mathrm{Ca}) (V_{\mathrm{d}} - V_{\mathrm{K}}) \\
I_{\text{K-AHP}}(V_{\mathrm{d}}, \mathrm{Ca}) &= \overline{g}_{\text{K-AHP}} q (V_{\mathrm{d}} - V_{\mathrm{K}})
\end{aligned}
$$

The kinetic equation for each of the gating variables h, n, s, c and q takes the form

$$
\frac{dy}{dt} = \frac{(y_{\infty}(U) - y)}{\tau_{y}(U)}
$$

The argument U equals V_{s} when $y = h, n$; V_{d} when $y = s, c$; and Ca when $y = q$. The steady state and time constant for each gating variable are derived from functions α_y, β_y, where $y_{\infty} = \alpha_y/(\alpha_y + \beta_y)$ and $\tau_y = 1/(\alpha_y + \beta_y)$. These functions for each gating variable are

$$
\begin{aligned}
\alpha_{\mathrm{m}} &= \frac{0.32(13.1 - V_{\mathrm{s}})}{\exp((13.1 - V_{\mathrm{s}})/4) - 1} \\
\beta_{\mathrm{m}} &= \frac{0.28(V_{\mathrm{s}} - 40.1)}{\exp((V_{\mathrm{s}} - 40.1)/5) - 1} \\
\alpha_{\mathrm{n}} &= \frac{0.016(35.1 - V_{\mathrm{s}})}{\exp((35.1 - V_{\mathrm{s}})/5) - 1} \\
\beta_{\mathrm{n}} &= 0.25 \exp(0.5 - 0.025 V_{\mathrm{s}}) \\
\alpha_{\mathrm{h}} &= 0.128 \exp((17 - V_{\mathrm{s}})/18) \\
\beta_{\mathrm{h}} &= \frac{4}{1 + \exp((40 - V_{\mathrm{s}})/5)} \\
\alpha_{\mathrm{s}} &= \frac{1.6}{1 + \exp(-0.072(V_{\mathrm{d}} - 65))}
\end{aligned}
$$

$$\beta_s = \frac{0.02(V_d - 51.1)}{\exp((Vd - 51.1)/5) - 1}$$
$$\alpha_c = \frac{\exp((V_d - 10)/11) - \exp((V_d - 6.5)/27)}{18.975} \text{ for } V_d \leq 50$$
$$\alpha_c = 2\ \exp((6.5 - V_d)/27) \text{ for } V_d > 50$$
$$\beta_c = 2\ \exp((6.5 - V_d)/27) - \alpha_c \text{ for } V_d \leq 50$$
$$\beta_c = 0 \text{ for } V_d > 50$$
$$\alpha_q = \min((0.00002)\text{Ca}, 0.01)$$
$$\beta_q = 0.001$$

The sodium current activates instantaneously ($m \equiv m_\infty(V_s)$).

These equations are supplemented by an equation for Ca^{2+} handling in the dendritic compartment,

$$\frac{d\text{Ca}}{dt} = -0.13 I_{\text{Ca}} - 0.075\text{Ca}$$

All other parameter values for these equations are listed in Table 1.

Table 1 Parameter values CA3 pyramidal cell model

Mechanism	CA3 pyramidal cell
Leak conductance ($\overline{g}_L$) (mS/cm^2)	0.1
Sodium ($\overline{g}_{\text{Na}}$) (mS/cm^2)	30
Delayed rectifier K^+ ($\overline{g}_{\text{K-DR}}$) (mS/cm^2)	15
Calcium ($\overline{g}_{\text{Ca}}$) (mS/cm^2)	10
Ca-activated potassium ($\overline{g}_{K-C}$) (mS/cm^2)	15
Potassium afterhyperpolarization ($\overline{g}_{\text{K-AHP}}$) (mS/cm^2)	0.8
$\overline{g}_{\text{NMDA}}$ (mS/cm^2)	0.0
$\overline{g}_{\text{AMPA}}$ (mS/cm^2)	0.0
V_{Na} (mV)	120
V_{Ca} (mV)	140
V_{K} (mV)	−15
V_{L} (mV)	0
V_{Syn} (mV)	60
I_s (μA/cm^2)	−0.5
I_d (μA/cm^2)	0.0
g_c (mS/cm^2)	2.1
$p(\text{area}_d/\text{area}_s)$	0.5
C_m (μF/cm^2)	3

Basket Cell Model

The basket cell (BC) is a five-compartment cell (Santhakumar et al., 2005) comprised of a soma (length = 20 μm, diameter = 4 μm), two apical dendritic compartments (length = 75 μm, diameter reduces outwards from the cell body through

sub-compartments 1–4) and two basal dendritic compartments (length $= 50\,\mu$m, diameter reduces outwards from the cell body through sub-compartments 1–4). The reduction in diameter simulates the increase in resistance of the outer regions of the dendrite where a current injection of a larger value would be required to activate the cell's firing properties in the soma. Details of the active membrane properties are given below in Appendix 2, in the specification for the basket cell used in the CA1 model.

AMPA and GABA Synapse Models

Excitatory AMPA synapses onto PCs and BCs have a conductance with instantaneous rise time and an exponential decay with time constant 0.1 ms, a current reversal potential of 5 mV and a synaptic delay of 0.33 ms. The GABA-A synapses from the BCs onto the PCs have a conductance with a dual exponential waveform with rise time of 1 ms and decay time of 7 ms, a current reversal potential of -75 mV and a synaptic delay of 2 ms. The maximum conductance for each synaptic pathway for the different network configurations is given in Table 2.

Table 2 Maximum synaptic conductances (μS) in CA3 models

Model	PC-PC AMPA	PC-BC AMPA	GABA-A
Pseudo inhibition	0.0154	–	0.00017
1 basket cell	0.014	0.05	0.01
100 basket cells	0.014	0.18	0.003

Appendix 2: CA1 Cell Models

Pyramidal Cell Model

The geometry of the pyramidal cell, and for the other cell models for CA1, is given in Table 3. The active properties of the PC are derived from the model of Poirazi (see the on-line supplement to Poirazi et al., 2003a, b and Pissadaki and Poirazi, this volume). The somatic (s), axonic (a) and radiatum (rad), lacunosum-moleculare (LM) and oriens (ori) dendritic compartments of pyramidal cells obey the following current balance equations:

$$C\frac{dV_{\mathrm{s}}}{dt} = -I_{\mathrm{L}} - I_{\mathrm{Na}} - I_{\mathrm{K-DR}} - I_{\mathrm{A}} - I_{\mathrm{M}} - I_{\mathrm{h}} - I_{\mathrm{sAHP}} - I_{\mathrm{mAHP}} - I_{\mathrm{CaL}} - I_{\mathrm{CaT}} - I_{\mathrm{CaR}} - I_{\mathrm{buff}} - I_{\mathrm{syn}}$$

$$C\frac{dV_{\mathrm{a}}}{dt} = -I_{\mathrm{L}} - I_{\mathrm{Na}} - I_{\mathrm{K-DR}} - I_{\mathrm{M}} - I_{\mathrm{syn}}$$

Table 3 Structure of CA1 model cells

Dimensions	Pyramidal cell	Axo-axonic cell	Basket cell	Bistratified cell	OLM cell
Soma					
Diameter (μm)	10	10	10	10	10
Length (μm)	10	20	20	20	20
Total number of compartments (soma + dendritic compartments)	15	17	17	13	4
Dendritic compartments and dimensions (diameter × length, μm^2)					
Basal dendrite					3 × 250
Axon	1 × 150				1.5 × 150
Thick proximal SR dendrite	4 × 100				
Thick medium SR dendrite	3 × 100				
Thick distal SR dendrite	2 × 200				
Proximal SO dendrite	2 × 100				
Distal SO dendrite	1.5 × 200				
Thick SLM dendrite	2 × 100				
Medium SLM dendrite	1.5 × 100				
Thin SLM dendrite	1 × 50				
Thick SR dendrite		4 × 100	4 × 100	4 × 100	
Medium SR dendrite		3 × 100	3 × 100	3 × 100	
Thin SR dendrite		2 × 200	2 × 200	2 × 200	
Medium SLM dendrite		1.5 × 100	1.5 × 100		
Thin SLM dendrite		1 × 100	1 × 100		
Thick SO dendrite		2 × 100	2 × 100	2 × 100	
Medium SO dendrite		1.5 × 100	1.5 × 100	1.5 × 100	
Thin SO dendrite		1 × 100	1 × 100	1 × 100	

$$C\frac{dV_{\mathrm{rad,ori}}}{dt} = -I_{\mathrm{L}} - I_{\mathrm{Na}} - I_{\mathrm{K-DR}} - I_{\mathrm{A}} - I_{\mathrm{M}} - I_{\mathrm{h}} - I_{\mathrm{sAHP}} - I_{\mathrm{mAHP}} - I_{\mathrm{CaL}} - I_{\mathrm{CaT}} - I_{\mathrm{CaR}} - I_{\mathrm{buff}} - I_{\mathrm{syn}}$$

$$C\frac{dV_{\mathrm{LM}}}{dt} = -I_{\mathrm{L}} - I_{\mathrm{Na}} - I_{\mathrm{K-DR}} - I_{\mathrm{A}} - I_{\mathrm{syn}}$$

where I_{L} is the leak current, I_{Na} is the fast sodium current, $I_{\mathrm{K-DR}}$ is the delayed rectifier potassium current, I_{A} is the A-type K^+ current, I_{M} is the M-type K^+ current, I_{h} is a hyperpolarizing h-type current, I_{CaL}, I_{CaT} and I_{CaR} are the L-, T- and R-type Ca^{2+} currents, respectively, I_{sAHP} and I_{mAHP} are slow and medium Ca^{2+}-activated K^+ currents, I_{buff} is a calcium pump/buffering mechanism and I_{syn} is the synaptic

current. The conductance and reversal potential values for all ionic currents are listed in Table 4.

The sodium current is described by

$$I_{\mathrm{Na}} = \overline{g}_{\mathrm{Na}} \cdot m^2 \cdot h \cdot s \cdot (V - E_{\mathrm{Na}})$$

where an additional variable "s" is introduced to account for dendritic location-dependent slow attenuation of the sodium current.

Activation and inactivation kinetics for $\mathrm{I_{Na}}$ are given by

$$\begin{aligned} m_{t+dt} &= m_t + \left(1 + \exp -\frac{dt}{\tau_{\mathrm{m}}}\right) \cdot (m_{\mathrm{inf}} - m_t), \\ m_{\mathrm{inf}} &= \frac{1}{1 + \exp\left(-\frac{V+40}{3}\right)} \\ h_{t+dt} &= h_t + \left(1 - \exp\left(-\frac{dt}{\tau_{\mathrm{h}}}\right)\right) \cdot (h_{\mathrm{inf}} - h_t) \end{aligned}$$

$$\begin{aligned} h_{\mathrm{inf}} &= \frac{1}{1 + e\left(\frac{V+45}{3}\right)} \\ s_{t+dt} &= s_t + \left(1 + \exp\left(-\frac{dt}{\tau_\sigma}\right)\right) \cdot (s_{\mathrm{inf}} - s_t), \\ s_{\mathrm{inf}} &= \frac{1 + \mathrm{Na_{att}} \cdot \exp\left(\frac{V+60}{2}\right)}{1 + \exp\left(\frac{V+60}{2}\right)} \end{aligned}$$

with $dt = 0.1$ ms and time constants $\tau_{\mathrm{m}} = 0.05$ ms, $\tau_{\mathrm{h}} = 0.5$ ms, and

$$\tau_\sigma = \frac{0.00333(\mathrm{ms}) \cdot e^{0.0024(1/\mathrm{mV}) \cdot (V+60) \cdot Q(^\circ\mathrm{C})}}{1 + e^{0.0012(1/\mathrm{mV}) \cdot (V+60) \cdot Q(^\circ\mathrm{C})}}$$

The function $Q(^\circ\mathrm{C})$ is given by

$$Q(^\circ\mathrm{C}) = \frac{F}{R \cdot (T + ^\circ\mathrm{C})}$$

where $R = 8.315\,\mathrm{J}/^\circ\mathrm{C}$, $F = 9.648 \times 10^4$ Coul, $T = 273.16$ in Kelvin and $^\circ$C is the temperature in degrees Celsius. The $\mathrm{Na_{att}}$ variable represents the degree of sodium current attenuation and varies linearly from soma to distal trunk ($\mathrm{Na_{att}}\,\varepsilon[0 \rightarrow 1]$: maximum $\rightarrow$ zero attenuation).

The delayed rectifier current is given by

Table 4 Passive parameters and active ionic conductances of channels for all compartments of pyramidal model cells

Mechanism	Soma	Axon	OriProx	OriDist	RadProx	RadMed	RadDist	LM
C_m ($\mu F/cm^2$)	1	1	1	1	1	1	1	1
R_m (Ωcm^2)	20,000	20,000	20,000	20,000	20,000	20,000	20,000	20,000
R_a (Ωcm)	150	150	150	150	150	150	150	150
Leak conductance (S/cm^2)	0.0002	0.000005	0.000005	0.000005	0.000005	0.000005	0.000005	0.000005
Sodium conductance (S/cm^2)	0.007	0.1	0.007	0.007	0.007	0.007	0.007	0.007
Delayed rectifier K^+ conductance (S/cm^2)	0.0014	0.02	0.000868	0.000868	0.000868	0.000868	0.000868	0.000868
Proximal A-type K^+ conductance (S/cm^2)	0.0075	–	0.0075	0.0075	0.015	0	0	–
Distal A-type K^+ conductance (S/cm^2)	–	–	0	0	0	0.03	0.045	0.049
M-type K^+ conductance (S/cm^2)	0.06	0.03	0.06	0.06	0.06	0.06	0.06	–
I_h conductance (S/cm^2)	0.00005	–	0.00005	0.0001	0.0001	0.0002	0.00035	–
$V_{half,h}$ (mV)	−73	–	−81	−81	−82	−81	−81	–

Table 4 (continued)

Mechanism	Soma	Axon	OriProx	OriDist	RadProx	RadMed	RadDist	LM
L-type Ca^{2+} conductance (S/cm^2)	0.0007	–	0.000031635	0.000031635	0.000031635	0.0031635	0.0031635	–
T-type Ca^{2+} conductance (S/cm^2)	0.00005	–	0.0001	0.0001	0.0001	0.0001	0.0001	–
R-type Ca^{2+} conductance (S/cm^2)	0.0003	–	0.00003	0.00003	0.00003	0.00003	0.00003	–
Ca^{2+}-dependent sAHP K^+ conductance (S/cm^2)	0.0005	–	0.0005	0.0005	0.0005	0.0005	0.0005	–
Ca^{2+}-dependent mAHP K^+ conductance (S/cm^2)	0.09075	–	0.033	0.033	0.033	0.033	0.0041	–
E_L (mV)	−70	−70	−70	−70	−70	−70	−70	−70
E_{Na} (mV)	50	50	50	50	50	50	50	50
E_h, (mV)	−10	–	−10	−10	−10	−10	−10	−10
E_{Ca}, (mV)	140	–	140	140	140	140	140	–
E_K (mV)	−80	−80	−80	−80	−80	−80	−80	−80

$$I_{\mathrm{K-DR}} = \overline{g}_{\mathrm{K-DR}} \cdot m^2 \cdot (V - E_{\mathrm{K}})$$
$$m_{t+dt} = m_t + \left(1 - \exp\left(-\frac{dt}{2.2}\right)\right) \cdot (m_{\mathrm{inf}} - m_t),$$
$$m_{\mathrm{inf}} = \frac{1}{1 + \exp\left(-\frac{V+42}{2}\right)}$$

The sodium and delayed rectifier channel properties are slightly different in the soma, axon and dendritic arbor. To fit experimental data regarding the backpropagation of spike trains, soma and axon compartments have a lower threshold for Na^+ spike initiation (≈ -57 mV) than dendritic ones (≈ -50 mV). Thus, the m_{inf} and h_{inf} somatic/axonic HH channel kinetics as well as the time constants for both $I^{\mathrm{sa}}_{\mathrm{Na}}$and $I^{\mathrm{sa}}_{\mathrm{K-DR}}$ are modified as follows. For the sodium

$$m^{\mathrm{sa}}_{\mathrm{inf}} = \frac{1}{1 + \exp\left(-\frac{V+44}{3}\right)},$$
$$h^{\mathrm{sa}}_{\mathrm{inf}} = \frac{1}{1 + \exp\left(\frac{V+49}{3.5}\right)}$$

while for the potassium delayed rectifier

$$m^{\mathrm{sa}}_{\mathrm{inf}} = \frac{1}{1 + \exp\left(-\frac{V+46.3}{3}\right)}$$

The somatic time constant for somatic/axonic Na^+ channel activation is kept the same $\tau_{\mathrm{m}} = 0.05$ ms while for inactivation is set to $\tau_{\mathrm{h}} = 1$ ms. The τ value for the delayed rectifier channel activation is set to $\tau_{\mathrm{m}} = 3.5$ ms. In all of the following equations, τ values are given in ms.

The fast inactivating A-type K^+ current is described by

$$I_{\acute{\mathrm{A}}} = \overline{g}_{\mathrm{A}} \cdot n_{\mathrm{A}} \cdot l \cdot (V - E_{\mathrm{K}})$$
$$n_{\mathrm{A}}(t+1) = n_{\mathrm{A}}(t) + (n_{A_\infty} - n_{\mathrm{A}}(t)) \cdot (1 - e^{-dt/\tau_{\mathrm{n}}})$$

where $\tau_{\mathrm{n}} = 0.2$ ms

$$n_{\mathrm{A}_\infty} = \frac{\alpha_{\mathrm{n_A}}}{\alpha_{\mathrm{n_A}} + \beta_{\mathrm{n_A}}}$$
$$\alpha_{\mathrm{n_A}} = \frac{-0.01(V + 21.3)}{e^{-(V+21.3)/35} - 1}, \qquad \beta_{\mathrm{n_A}} = \frac{0.01(V + 21.3)}{e^{(V+21.3)/35} - 1}$$
$$l(t+1) = l(t) + (l_\infty - l(t)) \cdot (1 - e^{-dt/\tau_{\mathrm{l}}})$$
$$l_\infty = \frac{\alpha_{\mathrm{l}}}{\alpha_{\mathrm{l}} + \beta_{\mathrm{l}}}$$
$$\alpha_{\mathrm{l}} = \frac{-0.01(V + 58)}{e^{(V+58)/8.2} - 1}, \qquad \beta_{\mathrm{l}} = \frac{0.01(V + 58)}{e^{-(V+58)/8.2} - 1}$$

where $\tau_l = 5 + 2.6(V + 20)/10$, if $V > 20\,\text{mV}$ and $\tau_l = 5$, elsewhere.

The hyperpolarizing h-current is given by

$$
\begin{aligned}
&I_h = g_h \cdot tt \cdot (V - E_h)\\
&\frac{dtt}{dt} = \frac{tt_\infty - tt}{\tau_{tt}}\\
&tt_\infty = \frac{1}{1 + e^{-(V - V_{half})/k_l}}, \qquad \tau_{tt} = \frac{e^{0.0378 \cdot \varsigma \cdot gmt \cdot (V - V_{halft})}}{qtl \cdot q10^{(T-33)/10} \cdot a0t \cdot (1 + a_{tt})}\\
&a_{tt} = e^{0.00378 \cdot \varsigma \cdot (V - V_{halft})}
\end{aligned}
$$

where ζ, gmt, $q10$ and qtl are 2.2, 0.4, 4.5 and 1, respectively, $a0t$ is 0.0111 1/ms, $V_{halft} = -75\,\text{mV}$ and $k_l = -8$.

The slowly activating voltage-dependent potassium current, I_M, is given by the equations:

$$
\begin{aligned}
&I_m = 10^{-4} \cdot T_{adj}(^\circ\text{C}) \cdot \overline{g}_m \cdot m \cdot (V - E_K)\\
&T_{adj}(^\circ\text{C}) = 2.3^{(^\circ\text{C}-23)/10}\\
&m_{t+dt} = m_t + \left(1 - e\left(-\frac{dt \cdot T_{adj}(^\circ\text{C})}{\tau}\right)\right) \cdot \left(\frac{\alpha(V)}{(\alpha(V) + \beta(V)} - m_t\right)\\
&\alpha(V) = 10^{-3} \cdot \frac{(V + 30)}{(1 - e^{-(V+30)/9})}\\
&\beta(V) = -10^{-3} \cdot \frac{(V + 30)}{(1 - e^{(V+30)/9})}\\
&\tau = \frac{1}{\alpha(V) + \beta(V)}
\end{aligned}
$$

The slow afterhyperpolarizing current, I_{sAHP}, is given by

$$
\begin{aligned}
&I_{sAHP} = \overline{g}_{sAHP} \cdot m^3 \cdot (V - E_K)\\
&\frac{dm}{dt} = \frac{\frac{\text{Cac}}{(1+\text{Cac})} - m}{\tau}\\
&\tau = \max\left(\frac{1}{0.003(1/\text{ms}) \cdot (1 + \text{Cac}) \cdot 3^{(^\circ\text{C}-22)/10}}, 0.5\right)
\end{aligned}
$$

where $\text{Cac} = (\text{Ca}_{in}/0.025(\text{mM}))^2$.

The medium afterhyperpolarizing current, I_{mAHP}, is given by

$$
\begin{aligned}
I_{\mathrm{mAHP}} &= \overline{g}_{\mathrm{mAHP}} \cdot m \cdot (V - E_{\mathrm{K}}) \\
m_{t+dt} &= m_t + \left(1 + \exp\left(-\frac{dt}{\tau_{\mathrm{m}}}\right)\right) \cdot \left(\frac{\alpha_{\mathrm{m}}(V)}{\tau_{\mathrm{m}}} - m_t\right) \\
\alpha_{\mathrm{m}}(V) &= \frac{0.48(1/\mathrm{ms})}{1 + \frac{0.18(\mathrm{mM})}{\mathrm{Ca_{in}}} \cdot e^{(-1.68 \cdot V \cdot Q(^\circ\mathrm{C}))}} \\
\beta_{\mathrm{m}}(V) &= \frac{0.28(1/\mathrm{ms})}{1 + \frac{\mathrm{Ca_{in}}}{0.011(\mathrm{mM}) \cdot e^{(-2 \cdot V \cdot Q(^\circ\mathrm{C}))}}} \\
\tau_{\mathrm{m}} &= \frac{1}{\alpha_{\mathrm{m}}(V) + \beta_{\mathrm{m}}(V)}
\end{aligned}
$$

The somatic high-voltage-activated (HVA) L-type Ca^{2+} current is given by

$$
\begin{aligned}
I^s_{\mathrm{CaL}} &= \overline{g}^s_{\mathrm{CaL}} \cdot m \cdot \frac{0.001\,\mathrm{mM}}{0.001\,\mathrm{mM} + \mathrm{Ca_{in}}} \cdot ghk(V, \mathrm{Ca_{in}}, \mathrm{Ca_{out}}) \\
\alpha_{\mathrm{m}}(V) &= -0.055 \cdot \frac{(V + 27.01)}{e^{-(V+27.01)/3.8} - 1} \\
\beta_{\mathrm{m}}(V) &= 0.94 \cdot e^{-(V+63.01)/17} \\
\tau_{\mathrm{m}} &= \frac{1}{5(\alpha_{\mathrm{m}}(V) + \beta_{\mathrm{m}}(V))}
\end{aligned}
$$

whereas the dendritic L-type calcium channels have different kinetics:

$$
\begin{aligned}
I^d_{\mathrm{CaL}} &= \overline{g}^d_{\mathrm{CaL}} \cdot m^3 \cdot h \cdot (V - E_{\mathrm{Ca}}) \\
\alpha(V) &= \frac{1}{1 + e^{-(V+37)}}, \beta(V) = \frac{1}{1 + e^{(V+41)/0.5}}
\end{aligned}
$$

Their time constants are equal to $\tau_{\mathrm{m}} = 3.6\,\mathrm{ms}$ and $\tau_{\mathrm{h}} = 29\,\mathrm{ms}$.
The low-voltage-activated (LVA) T-type Ca^{2+} channel kinetics are given by

$$
\begin{aligned}
I_{\mathrm{CaT}} &= \overline{g}_{\mathrm{CaT}} \cdot m^2 \cdot h \frac{0.001\,\mathrm{mM}}{0.001\,\mathrm{mM} + \mathrm{Ca_{in}}} \cdot ghk(V, \mathrm{Ca_{in}}, \mathrm{Ca_{out}}) \\
ghk(V, \mathrm{Ca_{in}}, \mathrm{Ca_{out}}) &= -x \cdot (1 - \tfrac{\mathrm{Ca_{in}}}{\mathrm{Ca_{out}}} \cdot e^{V/x}) \cdot f(V/x) \\
x &= \frac{0.0853 \cdot (T + ^\circ\mathrm{C})}{2}, \quad f(z) = \begin{cases} 1 - \frac{z}{2} & \text{if abs(z)} < 10^{-4} \\ \frac{z}{e^z - 1} & \text{otherwise} \end{cases}
\end{aligned}
$$

$$m_{t+dt} = m_t + (1 + e^{-dt/\tau_m}) \cdot \left(\frac{\alpha_{m(V)}}{\alpha_m(V) + \beta_m(V)} - m_t \right)$$
$$h_{t+dt} = h_t + (1 - e^{-dt/\tau_h}) \cdot \left(\frac{\alpha_h(V)}{\alpha_h(V) + \beta_h(V)} - h_t \right)$$
$$\alpha_m(V) = -0.196 \cdot \frac{(V - 19.88)}{e^{-(V-19.88)/10} - 1}, \beta_m(V) = 0.046 \cdot e^{-(V/22.73)}$$
$$\alpha_h(V) = 0.00016 \cdot e^{-(V+57)/19}, \beta_h(V) = \frac{1}{e^{-(V-15)/10} + 1}$$
$$\tau_m = \frac{1}{\alpha_m(V) + \beta_m(V)}, \tau_h = \frac{1}{0.68 \cdot (\alpha_h(V) + \beta_h(V)}$$

where Ca_{in} and Ca_{out} are the internal and external calcium concentrations. The HVA R-type Ca^{2+} current is described by

$$I_{CaR} = \overline{g}_{CaR} \cdot m^3 \cdot h \cdot (V - E_{Ca})$$
$$m_{t+dt} = m_t + (1 + e^{-dt/\tau_m}) \cdot (\alpha(V) - m_t)$$
$$h_{t+dt} = h_t + (1 - e^{-dt/\tau_h}) \cdot (\beta(V) - h_t)$$

The difference between somatic and dendritic CaR currents lies in the $\alpha(V)$, $\beta(V)$ and τ parameter values. For the somatic current, $\tau_m = 100\,\text{ms}$ and $\tau_h = 5\,\text{ms}$ while for the dendritic current $\tau_m = 50\,\text{ms}$ and $\tau_h = 5\,\text{ms}$. The $\alpha(V)$ and $\beta(V)$ equations for dendritic CaR channels are

$$\alpha(V) = \frac{1}{1 + e^{-(V+48.5)/3}}, \beta(V) = \frac{1}{1 + e^{(V+53)}}$$

while for the somatic CaR channels

$$\alpha(V) = \frac{1}{1 + e^{-(V+60)/3}}, \beta(V) = \frac{1}{1 + e^{(V+62)}}$$

Finally, a calcium pump/buffering mechanism is inserted at the cell body and along the apical and basal trunk. The kinetic equations are given by (where $f_e = 10,000/18$)

$$\text{drive\_channel} = \begin{cases} -f_e \cdot \frac{I_{Ca}}{0.2 \cdot F} & \text{if drive\_channel} > 0\,\text{mM/ms} \\ 0 & \text{otherwise} \end{cases}$$
$$\frac{d\text{Ca}}{dt} = \text{drive\_channel} + \frac{(10^{-4}(\text{mM}) - \text{Ca})}{7 \cdot 200\,(\text{ms})}$$

Axo-axonic, Basket and Bistratified Cell Models

Active properties of these cells are derived from the interneuron model of Santhakumar et al. (2005). All compartments obey the following current balance equation:

$$C_m \frac{dV}{dt} = I_{\text{ext}} - I_{\text{L}} - I_{\text{Na}} - I_{\text{K-DR,fast}} - I_{\text{A}} - I_{\text{CaL}} - I_{\text{CaN}} - I_{\text{AHP}} - I_{\text{C}} - I_{\text{syn}}$$

where C_m is the membrane capacitance, V is the membrane potential, I_{L} is the leak current, I_{Na} is the sodium current, $I_{\text{K-DR,fast}}$ is the fast delayed rectifier K^+ current, I_{A} is the A-type K^+ current, I_{CaL} is the L-type Ca^{2+} current, I_{CaN} is the N-type Ca^{2+} current, I_{AHP} is the Ca^{2+}-dependent K^+ (SK) current, I_{C} is the Ca^{2+} and voltage-dependent K^+ (BK) current and I_{syn} is the synaptic current. The conductance and reversal potential values of all ionic currents are listed in Table 5.

Table 5 Passive parameters and active ionic conductances of channels for all compartments of axo-axonic, basket and bistratified model cells

Mechanism	Axo-axonic cell	Basket cell	Bistratified cell
C_m (μF/cm^2)	1.4	1.4	1.4
R_a (Ωcm)	100	100	100
Leak conductance (S/cm^2)	0.00018	0.00018	0.00018
Sodium (S/cm^2)	0.15	0.2	0.3
Delayed rectifier K^+ (S/cm^2)	0.013	0.013	0.013
A-type K^+ (S/cm^2)	0.00015	0.00015	0.00015
L-type Ca^{2+} (S/cm^2)	0.005	0.005	0.005
N-type Ca^{2+} (S/cm^2)	0.0008	0.0008	0.0008
Ca^{2+}-dependent K^+ (S/cm^2)	0.000002	0.000002	0.000002
Ca^{2+}- and voltage-dependent K^+ (S/cm^2)	0.0002	0.0002	0.0002
Time constant for decay of intracellular Ca^{2+} (ms)	10	10	10
Steady-state intracellular Ca^{2+} concentration (μM)	$5.e^{-6}$	$5.e^{-6}$	$5.e^{-6}$
E_{Na} (mV)	55	55	55
E_{K} (mV)	-90	-90	-90
E_{Ca} (mV)	130	130	130
E_{L} (mV)	-60	-60	-60
$[Ca^{2+}]_0$ (μM)	2	2	2

The sodium current and its kinetics are described by

$$I_{\text{Na}} = g_{\text{Na}} m^3 h (V - E_{\text{Na}})$$
$$\frac{dm}{dt} = \alpha_{\text{m}}(1 - m) - \beta_{\text{m}} m,\ \alpha_{\text{m}} = \frac{-0.3(V - 25)}{(1 - e^{(V-25)/-5})},\ \beta_{\text{m}} = \frac{0.3(V - 53)}{(1 - e^{(V-53)/5})}$$
$$\frac{dh}{dt} = \alpha_{\text{h}}(1 - h) - \beta_{\text{h}} h,\ \alpha_{\text{h}} = \frac{0.23}{e^{(V-3)/20}},\ \beta_{\text{h}} = \frac{3.33}{(1 + e^{(V-55.5)/-10})}$$

The fast delayed rectifier K^+ current, $I_{\text{K-DR,fast}}$, is given by

$$I_{\mathrm{K-DR,fast}} = g_{\mathrm{K-DR,fast}} n_{\mathrm{f}}^4 (V - E_{\mathrm{K}})$$
$$\frac{dn_{\mathrm{f}}}{dt} = \alpha_{\mathrm{n_f}}(1 - n_{\mathrm{f}}) - \beta_{\mathrm{n_f}} n_{\mathrm{f}}$$
$$\alpha_{\mathrm{n_f}} = \frac{-0.07(V - 47)}{(1 - e^{(V-47)/-6})}$$
$$\beta_{\mathrm{n_f}} = 0.264\, e^{(V-22)/4}$$

The N-type Ca^{2+} current, I_{CaN}, is given by

$$I_{\mathrm{CaN}} = g_{\mathrm{CaN}} c^2 d (V - E_{\mathrm{Ca}})$$
$$\frac{dc}{dt} = \alpha_{\mathrm{c}}(1 - c) - \beta_{\mathrm{c}} c,\ \alpha_{\mathrm{c}} = \frac{0.19(19.88 - V)}{(e^{(19.88-V)/10} - 1)},\ \beta_{\mathrm{c}} = 0.046 e^{-V/20.73}$$
$$\frac{dd}{dt} = \alpha_{\mathrm{d}}(1 - d) - \beta_{\mathrm{d}} d,\ \alpha_{\mathrm{d}} = 1.6 \cdot 10^{-4} e^{-V/48.4},\ \beta_{\mathrm{d}} = \frac{1}{(1 + e^{(39-V)/10})}$$

The Ca^{2+}-dependent K^+ (SK) current, I_{AHP}, is described by

$$I_{\mathrm{AHP}} = g_{\mathrm{AHP}} q^2 (V - E_{\mathrm{K}})$$
$$\frac{dq}{dt} = \alpha_{\mathrm{q}}(1 - q) - \beta_{\mathrm{q}} q$$

$$\alpha_{\mathrm{q}} = \frac{0.00246}{e^{(12 \cdot \log_{10}([\mathrm{Ca}^{2+}]) + 28.48)/-4.5}},\ \beta_{\mathrm{q}} = \frac{0.006}{e^{(12 \cdot \log_{10}([\mathrm{Ca}^{2+}]) + 60.4)/35}}$$

$$\frac{d[\mathrm{Ca}^{2+}]_{\mathrm{i}}}{dt} = B \sum_{T,N,L} I_{\mathrm{Ca}} - \frac{[\mathrm{Ca}^{2+}]_{\mathrm{i}} - [\mathrm{Ca}^{2+}]_0}{\tau}$$

where $B = 5.2 \cdot 10^{-6}/Ad$ in units of mol/(C m^3) for a shell of surface area A and thickness d (0.2 μm), and $\tau = 10$ ms was the calcium removal rate. $[\mathrm{Ca}^{2+}]_0 = 5\,\mu\mathrm{M}$ was the resting calcium concentration.

The Ca^{2+} and voltage-dependent K^+ (BK) current, I_{c}, is

$$I_{\mathrm{C}} = g_{\mathrm{c}} o (v - E_{\mathrm{K}})$$

where o is the activation variable (Migliore et al. J. Neurophysiol. 73:1157–1168, 1995). The A-type K^+ current, I_A, is described by

$$I_{\mathrm{A}} = g_{\mathrm{A}} ab(V - E_{\mathrm{k}})$$

$$\frac{da}{dt} = \alpha_{\mathrm{a}}(1 - a) - \beta_{\mathrm{a}} a$$

$$\alpha_{\mathrm{a}} = \frac{0.02(13.1 - V)}{e^{13.1 - V/10} - 1},\ \beta_{\mathrm{a}} = \frac{0.0175(V - 40.1)}{e^{V - 40.1/10} - 1}$$

$$\frac{db}{dt} = \alpha_{\mathrm{b}}(1 - b) - \beta_{\mathrm{b}} b$$

$$\alpha_{\mathrm{b}} = 0.0016\, e^{-13 - V/18},\ \beta_{\mathrm{b}} = \frac{0.05}{1 + e^{10.1 - V/5}}$$

The L-type Ca^{2+} current, I_{CaL}, is described by

$$I_{\mathrm{CaL}} = g_{\mathrm{CaL}} \cdot s_{\infty}^2 \cdot V \cdot \frac{1 - \frac{[\mathrm{Ca}^{2+}]_{\mathrm{i}}}{[\mathrm{Ca}^{2+}]_0} e^{2\mathrm{FV/kT}}}{1 - e^{2\mathrm{FV/kT}}}$$

where g_{CaL} is the maximal conductance, s_{∞} is the steady-state activation variable, F is Faraday's constant, T is the temperature, k is Boltzmann's constant, $[\mathrm{Ca}^{2+}]_0$ is the equilibrium calcium concentration and $[\mathrm{Ca}^{2+}]_{\mathrm{i}}$ is described above. The activation variable, s_{∞}, is then

$$s_{\infty} = \frac{\alpha_{\mathrm{s}}}{\alpha_{\mathrm{s}} + \beta_{\mathrm{s}}},\ \alpha_{\mathrm{s}} = \frac{15.69(-V + 81.5)}{e^{-V + 81.5/10} - 1},\ \beta_{\mathrm{s}} = 0.29 \cdot e^{-V/10.86}$$

OLM Cell Model

Active properties are derived from the model of Saraga et al. (2003). The somatic (s), axonic (a) and dendritic (d) compartments of each OLM cell obeyed the following current balance equations:

$$C_m \frac{dV_{\mathrm{s}}}{dt} = I_{\mathrm{ext}} - I_{\mathrm{L}} - I_{\mathrm{Na,s}} - I_{\mathrm{K,s}} - I_{\mathrm{A}} - I_{\mathrm{h}} - I_{\mathrm{syn}}$$

$$C_m \frac{dV_{\mathrm{d}}}{dt} = I_{\mathrm{ext}} - I_{\mathrm{L}} - I_{\mathrm{Na,d}} - I_{\mathrm{K,d}} - I_{\mathrm{A}} - I_{\mathrm{syn}}$$

$$C_m \frac{dV_{\mathrm{a}}}{dt} = I_{\mathrm{ext}} - I_{\mathrm{L}} - I_{\mathrm{Na,d}} - I_{\mathrm{K,d}}$$

The conductance and reversal potential values per compartment are listed in Table 6.

Table 6 Passive parameters and active ionic conductances of channels for all compartments of OLM model cells

	Compartment		
Mechanism	Soma	Dendrite	Axon
C_m ($\mu F/cm^2$)	1.3	1.3	1.3
R_a (Ωcm)	150	150	150
Leak conductance (S/cm^2)	0.00005	0.00005	0.00005
E_L (mV)	–70	–70	–70
Sodium (S/cm^2)	0.0107	0.0234	0.01712
E_{Na} (mV)	90	90	90
Delayed rectifier K^+ (S/cm^2)	0.0319	0.046	0.05104
E_K (mV)	–100	–100	–100
A-type K^+ (S/cm^2)	0.0165	0.004	–
E_A (mV)	–100	–100	–100
I_h (S/cm^2)	0.0005	–	–
E_h (mV)	–32.9	–32.9	–32.9

Table 7 Synaptic parameters

Mechanisms	AMPA	NMDA	GABA-A	GABA-B
Rise (ms)	0.5	2.3	1	35
Fall (ms)	3	100	8	100
Reversal potential (mV)	0	0	–75	–75

Table 8 Synaptic conductance parameters (in μS). Text in parenthesis signifies the type of postsynaptic receptor

		Postsynaptic					
		EC	CA3	Septum	Pyr	AAC	BC	BSC	OLM
Presynaptic	EC				0.001 (AMPA)	0.00015 (AMPA)	0.00015 (AMPA)	0.00015 (AMPA)	
	CA3				0.0005 (NMDA)	0.00015 (AMPA)	0.00015 (AMPA)	0.00015 (AMPA)	
	Septum					0.02 (GABA-A)	0.02 (GABA-A)		
	Pyr				0.001 (AMPA)	0.0005 (AMPA)	0.0005 (AMPA)	0.0005 (AMPA)	0.0005 (AMPA)
	AAC				0.04 (GABA-A)				
	BC				0.02 (GABA-A)	0.001 (GABA-A)		0.02 (GABA-A)	
	BSC				0.002 (GABA-A) 0.0004 (GABA-B)		0.01 (GABA-A)		
	OLM				0.04 (GABA-A) 0.0004 (GABA-B)		0.01 (GABA-A)		

The sodium current is described by

$$
\begin{aligned}
I_{\mathrm{Na}} &= g_{\mathrm{Na}} m^3 h (V - E_{\mathrm{Na}}) \\
\frac{dm}{dt} &= \alpha_{\mathrm{m}}(1 - m) - \beta_{\mathrm{m}} m \\
\frac{dh}{dt} &= \alpha_{\mathrm{h}}(1 - h) - \beta_{\mathrm{h}} h
\end{aligned}
$$

where m and h are the activation and inactivation variables, respectively. The forward and backward rate constants are described by

$$
\begin{aligned}
\alpha_{\mathrm{m,soma/axon}} &= \frac{-0.1(V + 38)}{\exp\left(\frac{-(V+38)}{10}\right) - 1}, \ \beta_{\mathrm{m,soma/axon}} = 4 \exp\left(\frac{-(V + 63)}{18}\right) \\
\alpha_{\mathrm{h,soma/axon}} &= 0.07 \exp\left(\frac{-(V + 63)}{20}\right), \ \beta_{\mathrm{h,soma/axon}} = \frac{1}{1 + \exp\left(\frac{-(V+33)}{10}\right)} \\
\alpha_{\mathrm{m,dend}} &= \frac{-0.1(V + 45)}{\exp\left(\frac{-(V+45)}{10}\right) - 1}, \ \beta_{\mathrm{m,dend}} = 4 \exp\left(\frac{-(V + 70)}{18}\right) \\
\alpha_{\mathrm{h,dend}} &= 0.07 \exp\left(\frac{-(V + 70)}{20}\right), \ \beta_{\mathrm{h,dend}} = \frac{1}{1 + \exp\left(\frac{-(V+40)}{10}\right)}
\end{aligned}
$$

The potassium current, I_{K}, is described by

$$
\begin{aligned}
I_{\mathrm{K}} &= g_{\mathrm{K}} n^4 (V - E_{\mathrm{K}}) \\
\frac{dn}{dt} &= \alpha_{\mathrm{n}}(1 - n) - \beta_{\mathrm{n}} n
\end{aligned}
$$

where n is the activation variable for this channel. The forward and backward constants are described by

$$
\begin{aligned}
\alpha_{\mathrm{n,soma/axon}} &= \frac{-0.018(V - 25)}{\exp\left(\frac{-(V-25)}{25}\right) - 1}, \ \beta_{\mathrm{n,soma/axon}} = \frac{0.0036(V - 35)}{\exp\left(\frac{V-35}{12}\right) - 1} \\
\alpha_{\mathrm{n,dend}} &= \frac{-0.018(V - 20)}{\exp\left(\frac{-(V-20)}{21}\right) - 1}, \ \beta_{\mathrm{n,soma/axon}} = \frac{0.0036(V - 30)}{\exp\left(\frac{V-30}{12}\right) - 1}
\end{aligned}
$$

The transient potassium current, I_A, is described by

$$I_A = g_A ab(V - E_k)$$
$$\frac{da}{dt} = \frac{(a_\infty - a)}{\tau_a},\ a_\infty = \frac{1}{\left(1 + \exp\left(\frac{-(V+14)}{16.6}\right)\right)},\ \tau_a = 5\,\text{ms} \quad \frac{db}{dt} = \frac{(b_\infty - b)}{\tau_b}$$
$$b_\infty = \frac{1}{\left(1 + \exp\left(\frac{-(V+71)}{7.3}\right)\right)},\ \tau_b = \frac{1}{\alpha_b - \beta_b}$$

where a and b are the activation and inactivation variables, respectively. The rate constants are given by

$$\alpha_b = \frac{0.000009}{\exp\left(\frac{V-26}{18.5}\right)},\ \beta_b = \frac{0.014}{0.2 + \exp\left(\frac{-(V+70)}{11}\right)}$$

The non-specific cation channel, I_h, is described by

$$I_h = g_h r(V - E_r)$$
$$\frac{dr}{dt} = \frac{(r_\infty - r)}{\tau_r}$$

where r is the activation variable for this channel. The steady-state activation curve and time constant are given by

$$r_\infty = \frac{1}{\left(1 + \exp\left(\frac{V+84}{10.2}\right)\right)},\ \tau_r = \frac{1}{\exp(-17.9 - 0.116V) + \exp(-1.84 + 0.09V)} + 100$$

Network Input Spike Trains

Septal cells: Septal cell output was modelled as bursts of action potentials using a presynaptic spike generator. A spike train consisted of bursts of action potentials at a mean frequency of 50 Hz for a half-theta cycle (125 ms; corresponding to a recall period) followed by a half-theta cycle of silence. Due to 40% noise in the interspike intervals, the 10 spike trains in the septal population were asynchronous.

Entorhinal cells (EC): EC cells were also modelled as noisy spike trains, using a presynaptic spike generator. A spike train consisted of spikes at an average gamma frequency of 40 Hz, but with individual spike times Gaussian-distributed around the regular ISI of 25 ms, with a standard deviation of 0.2. The population of EC inputs fired asynchronously.

CA3 pyramidal cells: CA3 pyramidal cells were modelled as spike trains of the same form and with the same characteristics (mean frequency and noise level) as the EC cells. Onset of CA3 firing was delayed by 9 ms relative to the EC trains to model the respective conduction delays of direct and trisynaptic loop inputs to CA1.

Further Reading

de Almeida, L., Idiart, M., and Lisman, J.E. (2007). Memory retrieval time and memory capacity of the CA3 network: role of gamma frequency oscillations. *Learning & Memory*, 14: 795–806.

Amaral, D. and Lavenex, P. (2007). Hippocampal neuroanatomy. In: *The Hippocampus Book* (eds. P. Andersen, R. Morris, D. Amaral, T. Bliss, and J. O'Keefe), Oxford: Oxford University Press, pp. 37–114.

Amaral, D. and Witter, M. (1989). The three-dimensional organization of the hippocampal formation: a review of anatomical data. *Neuroscience*, 31:571–591.

Amit, D. J. (1989). *Modeling Brain Function: The World of Attractor Neural Networks*. Cambridge: Cambridge University Press.

Axmacher, N., Mormann, F., Fernandez, G., Elger, C., and Fell, J. (2006). Memory formation by neuronal synchronization. *Brain Research Reviews*, 52:170–182.

Bartos, M., Vida, I., and Jonas, P. (2007). Synaptic mechanisms of synchronized gamma oscillations in inhibitory interneuron networks. *Nature Reviews Neuroscience*, 8:45–56.

Bliss, T., Collingridge, G., and Morris, R. (2007). Synaptic plasticity in the hippocampus. In: *The Hippocampus Book* (eds. P. Andersen, R. Morris, D. Amaral, T. Bliss, and J. O'Keefe), Oxford: Oxford University Press, chapter 10, pp. 343–474.

Brankack, J., Stewart, M., and Fox S. (1993). Current source density analysis of the hippocampal theta rhythm: associated sustained potentials and candidate synaptic generators. *Brain Research*, b15:310–327.

Brun, V.H., Otnass, M.K., Molden, S., Steffenach, H.A., Witter, M.P., Moser, M.B., and Moser, E.I. (2002). Place cells and place recognition maintained by direct entorhinal-hippocampal circuitry. *Science*, 296:2243–2246.

Buzsaki, G. and Chrobak, J. (1995). Temporal structure in spatially organized neuronal ensembles: a role for interneuronal networks. *Current Opinion in Neurobiology*, 5:504–510.

Cook, E.P. and Johnston, D. (1997). Active dendrites reduce location-dependent variability of synaptic input trains. *Journal of Neurophysiology*, 78:2116–2128.

Cutsuridis, V., Cobb, S., and Graham, B.P. (2008a). Encoding and retrieval in a CA1 microcircuit model of the hippocampus. In: *ICANN 2008*, LNCS 5164 (eds. V. Kurkova, R. Neruda, and J. Koutnik), Springer-Verlag Berlin Heidelberg, pp. 238–247.

Cutsuridis, V., Cobb, S., and Graham, B.P. (2008b). A Ca^{2+} dynamics model of the STDP symmetry-to-asymmetry transition in the CA1 pyramidal cell of the hippocampus. In: *ICANN 2008*, LNCS 5164 (eds. V. Kurkova, R. Neruda, and J. Koutnik), Springer-Verlag Berlin Heidelberg, pp. 627–635.

Cutsuridis, V., Cobb, S., and Graham B.P. (2009a). Encoding and retrieval in a model of the hippocampal CA1 microcircuit. *Hippocampus, DOI 10.1002/hipo.20661*, in press

Cutsuridis, V., Cobb, S., and Graham, B.P. (2009b). Modelling the STDP symmetry-to-asymmetry transition in the presence of GABAergic inhibition. *Neural Network World*, 19:471–481.

Cutsuridis, V., Cobb, S., and Graham, B.P. (2009c). How bursts shape the STDP curve in the presence/absence of GABA inhibition. In: *Artificial Neural Networks – ICANN 2009*, LNCS 5768, Springer Berlin Heidelberg, pp. 229–238.

Cutsuridis, V., Hunter, R., Cobb, S., and Graham B. P. (2007). Storage and recall in the CA1 microcircuit of the hippocampus: a biophysical model. *BMC Neuroscience* 8(Suppl 2): P33

Cutsuridis, V. and Wennekers, T (2009). Hippocampus, microcircuits and associative memory. *Neural Networks, Special issue: Neural Models of Cortical Microcircuits*, 22:1120–1128.

Freund, T. and Antal, M. (1988). GABA-containing neurons in the septum control inhibitory interneurons in the hippocampus. *Hippocampus*, 336:170–173.

Freund, T. and Buzsaki, G. (1996). Interneurons of the hippocampus. *Hippocampus*, 6:347–470.

Golding, N.L., Staff, N.P., and Spruston, N. (2002). Dendritic spikes as a mechanism for cooperative long-term potentiation. *Nature*, 418:326–331.

Graham, B.P. (2001). Pattern recognition in a compartmental model of a CA1 pyramidal cell. *Network: Computation in Neural Systems*, 12:473–492.

Graham, B.P. and Cutsuridis, V. (2009). Dynamical Information Processing in the CA1 Microcircuit of the Hippocampus. In: *Computational Modeling in Behavioral Neuroscience: Closing the Gap Between Neurophysiology and Behavior*. (eds. D. Heinke and E. Mavritasaki), pp. 1–20, London: Psychology Press, Taylor and Francis Group.

Guzowski, J.F., Knierim, J.J., and Moser, E.I. (2004). Ensemble dynamics of hippocampal regions CA3 and CA1. *Neuron*, 44:581–584.

Hasselmo, M., Bodelon, C., and Wyble, B. (2002a). A proposed function for hippocampal theta rhythm: separate phases of encoding and retrieval enhance reversal of prior learning. *Neural Computation*, 14:793–817.

Hasselmo, M., Hay, J., Ilyn, M., and Gorchetchnikov, A. (2002b). Neuromodulation, theta rhythm and rat spatial navigation. *Neural Networks*, 15:689–707.

Hopfield, J. (1982). Neural networks and physical systems with emergent collective computational abilities. *Proceedings of the National Academy of Science*, 79:2554–2558.

Hunter, R., Cobb, S., and Graham, B.P. (2008a). Improving recall in an associative neural network of spiking neurons. *Dynamic Brain - from Neural Spikes to Behaviors*, LNCS Vol. 5286, Springer, Berlin/Heidelberg, pp. 137–141.

Hunter, R., Cobb, S., and Graham, B.P. (2008b). Improving associative memory in a network of spiking neurons. *Artificial Neural Networks – ICANN 2008*, LNCS Vol. 5164, Springer, Berlin/Heidelberg, pp. 636–645.

Hunter, R., Cobb, S., and Graham, B.P. (2009). Improving associative memory in a network of spiking neurons. *Neural Network World*, 19:447–470.

Ishizuka, N., Weber, J., and Amaral, D. (1990). Organization of intrahippocampal projections originating from CA3 pyramidal cells in the rat. *Journal of Comparative Neurology*, 295:580–623.

Kali, S. and Freund, T.F. (2005). Distinct properties of two major excitatory inputs to hippocampal pyramidal cells: a computational study. *European Journal of Neuroscience*, 22:2027–2048.

Klausberger, T., Magill, P., Maki, G., Marton, L., Roberts, J., Cobden, P., Buzsaki, G., and Somogyi, P. (2003). Brain-state-and cell-type-specific firing of hippocampal interneurons in vivo. *Nature*, 421:844–848.

Klausberger, T., Marton, L., Baude, A., Roberts, J., Magill, P., and Somogyi, P. (2004). Spike timing of dendrite-targeting bistratified cells during hippocampal network oscillations in vivo. *Nature Neuroscience*, 7:41–47.

Klausberger, T., and Somogyi, P. (2008). Neuronal diversity and temporal dynamics: the unity of hippocampal circuit operations. *Science*, 321(5885):53–57.

Knierim, J.J., Lee, I., and Hargreaves, E.L.. (2006). Hippocampal place cells: parallel input streams, subregional processing, and implications for episodic memory. *Hippocampus*, 16:755–764.

Kunec, S., Hasselmo, M., and Kopell, N. (2005). Encoding and retrieval in the CA3 region of the hippocampus: a model of theta-phase separation. *Journal of Neurophysiology*, 94:70–82.

Lamsa, K., Heeroma, J., Somogyi, P., Rusakov, D., and Kullmann, D. (2007). Anti-Hebbian long-term potentiation in the hippocampal feedback circuit. *Science*, 315:1262–1266.

Leung, L., Roth, L., and Canning, K. (1995). Entorhinal inputs to hippocampal CA1 and dentate gyrus in the rat: a current-source-density study. *Journal of Neurophysiology*, 73: 2392–2403.

Levy, W.B. (1996). A sequence predicting CA3 is a flexible associator that learns and uses context to solve hippocampal-like tasks. *Hippocampus*, 6:579–590.

Li, X.G., Somogyi, P., Ylinen, A., and Buzaki, G. (1994). The hippocampal CA3 network: An in vivo intracellular labeling study. *Journal of Comparative Neurology*, 339:181–208.

Lisman, J. and Idiart, M. (1995). Storage of 7+-2 short-term memories in oscillatory subcycles. *Science*, 267:1512–1514.

Maccaferri, G. and Lacaille, J.-C. (2003). Hippocampal interneuron classifications -making things as simple as possible, not simpler. *Trends in Neuroscience*, 26:564–571.

Marr, D. (1971). A simple theory of archicortex. *Philosophical Transactions of the Royal Society of London. Series B, Biological Sciences*, 262(841): 23–81.

McNaughton, B.L. and Morris, R.G.M. (1987). Hippocampal synaptic enhancement and information storage within a distributed memory system. *TINS*, 10(10): 408–415.

Menschik E.D. and Finkel L.H. (1998). Neuromodulatory control of hippocampal function: towards a model of Alzheimer's disease. *Artificial Intelligence in Medicine*, 13: 99–121.

Migliore, M., Ferrante, M., and Ascoli, G.A. (2005). Signal propagation in oblique dendrites of CA1 pyramidal cells. *Journal of Neurophysiology*, 94:4145–4155.

Molyneaux, B.J. and Hasselmo ME. (2002). $GABA_B$ presynaptic inhibition has an in vivo time constant sufficiently rapid to allow modulation at theta frequency. *Journal of Neurophysiology*, 87:1196–1205.

Paulsen, O. and Moser, E. (1998). A model of hippocampal memory encoding and retrieval: GABAergic control of synaptic plasticity. *Trends in Neuroscience*, 21:273–279.

Pinsky, P. and Rinzel, J. (1994). Intrinsic and network rhythmogenesis in a reduced Traub model for CA2 neurons. *Journal of Computational Neuroscience*, 1:39–60.

Pissadaki, E. and Poirazi, P. (2007). Modulation of excitability in CA1 pyramidal neurons via the interplay of entorhinal cortex and CA3 inputs. *Neurocomputing*, 70:1735–1740.

Poirazi, P., Brannon, T., and Mel, B. (2003a). Arithmetic of subthreshold synaptic summation in a model CA1 pyramidal cell. *Neuron*, 37:977–987.

Poirazi, P., Brannon, T., and Mel, B. (2003b). Pyramidal neuron as a two-layer neural network. *Neuron*, 37:989–999.

Remondes, M. and Schuman, E. (2002). Direct cortical input modulates plasticity and spiking in CA1 pyramidal neurons. *Nature*, 416:736–740.

Santhakumar, V., Aradi, I., and Soltetz, I. (2005). Role of mossy fiber sprouting and mossy cell loss in hyperexcitability: a network model of the dentate gyrus incorporating cell types axonal typography. *Journal of Neurophysiology*, 93:437–453.

Saraga, F., Wu, C., Zhang, L., and Skinner, F. (2003). Active dendrites and spike propagation in multicompartmental models of oriens-lacunosum/moleculare hippocampal interneurons. *Journal of Physiology*, 552:673–689.

Sjostrom, P.J., Rancz, E.A., Roth, A., and Hausser, M. (2008). Dendritic excitability and synaptic plasticity. *Physiological Reviews*, 88:769–840.

Soleng, A.F., Raastad, M., and Andersen P. (2003). Conduction latency along CA3 hippocampal axons from rat. *Hippocampus*, 13:953–961.

Sommer, F. and Wennekers, T. (2000). Modelling studies on the computational function of fast temporal structure in cortical circuit activity. *Journal of Physiology (Paris)*, 94:473–488.

Sommer, F. and Wennekers, T. (2001). Associative memory in networks of spiking neurons. *Neural Networks*, 14:825–834.

Somogyi, P. and Klausberger, T. (2005). Defined types of cortical interneurone structure space and spike timing in the hippocampus. *Journal of Physiology*, 562.1:9–26.

Sun, H., Lyons, S., and Dobrunz, L. (2005). Mechanisms of target-cell specific short-term plasticity at Schaffer collateral synapses onto interneurones versus pyramidal cells in juvenile rats. *Journal of Physiology*, 568:815–840.

Treves, A. and Rolls, E. (1994). Computational analysis of the role of the hippocampus in memory. *Hippocampus*, 4:374–391.

Wallenstein, G. and Hasselmo, M. (1997). GABAergic modulation of hippocampal population activity: sequence learning, place field development, and the phase precession effect. *Journal of Neurophysiology*, 78:393–408.

Willshaw, D., Buneman, O., and Longuet-Higgins, H. (1969). Non-holographic associative memory. *Nature*, 222:960–962.

Wyble B.P., Linster C., and Hasselmo ME. (2000). Size of CA1-evoked synaptic potentials is related to theta rhythm phase in rat hippocampus. *Journal of Neurophysiology*, 83(4): 2138–44.